Manitoba
Energy and Mines
Geological Services

Economic Geology Report ER91-1

Results of a Rock Geochemical Study in the Area of the Rod Cu-Zn Deposit, Snow Lake, Manitobal

By K.J. Ferreira and M.A.F. Fedikow
Winnipeg, 1991

Energy and Mines

Hon. Harold J. Neufeld
Minister

Ian Haugh
Deputy Minister

Geological Services

W.D. McRitchie
Director

This publication is available in large print, audiotape or braille on request

recycled paper

92-03108/

ABSTRACT

Multiple, low contrast rock geochemical anomalies have been delineated in outcrop chip samples collected from a mapping grid constructed over the surface projection of the Rod Cu-Zn deposit. The areal extent of the anomalies and the limited range of concentrations for the halo-forming elements is probably related to the depth of burial and the attitude of the No. 2 ore zone. Broad correlations between bedrock, humus and vapour geochemical surveys are apparent.

TABLE OF CONTENTS

Page

ABSTRACT iii
INTRODUCTION 1
GEOLOGY 3
Regional Geology 3
Local Geology 3
Rod Deposit 3
Grid Area 3
SAMPLE COLLECTION, PREPARATION AND ANALYSIS 9
Results 9
GROUP 1 - Low Skewness and Kurtosis 11
Aluminum 11
Boron 11
Calcium 15
Cobalt 15
Copper 15
Magnesium 15
Nickel 15
Phosphorus 15
Potassium 15
Sodium 15
Strontium 15
Vanadium 15
GROUP 2 - Moderate Skewness or Kurtosis 15
Barium 15
Gold 15
Iron 15
Lead 15
Manganese 29
Zinc 28
GROUP 3 - High Skewness or Kurtosis 29
Arsenic 29
DISCUSSION AND CONCLUSIONS 33
Sulphide Selective Dissolution 33
Geochemical Anomalies 33
Rock, Humus and Vapour Surveys 33
CONCLUSIONS 35
ACKNOWLEDGMENTS 36
REFERENCES 37
APPENDIX I: Analytical data, rock geochemical samples, Rod deposit area 38
APPENDIX II: Histograms of analytical data for individual elements 40

FIGURES

Figure 1: General geology of the Flin Flon-Snow Lake greenstone belt (after Bailes, 1971) 2
Figure 2: Geology of part of the Snow Lake area (after Froese and Moore, 1980) 4
Figure 3: Stratigraphic sequence in the Amisk Group, Anderson Lake area, showing setting of the Lower Mine felsic unit (after Bailes *et al.*, 1987; nomenclature after Walford and Franklin, 1982) 5
Figure 4: Geology in the area of the vertical projection of the Rod Cu-Zn deposit 6
Figure 5: Grid map with sample numbers and locations 8
Figure 6: Contour map of Al (%) distribution in rock samples 12
Figure 7: Contour map of B (ppm) distribution in rock samples 13
Figure 8: Contour map of Ca (%) distribution in rock samples 14

Page

Figure 9: Contour map of Co (ppm) distribution in rock samples 16
Figure 10: Contour map of Cu (ppm) distribution in rock samples 17
Figure 11: Contour map of Mg (%) distribution in rock samples 18
Figure 12: Contour map of Ni (ppm) distribution in rock samples 19
Figure 13: Contour map of P (%) distribution in rock samples 20
Figure 14: Contour map of K (%) distribution in rock samples 21
Figure 15: Contour map of Na (%) distribution in rock samples 22
Figure 16: Contour map of Sr (ppm) distribution in rock samples 23
Figure 17: Contour map of V (ppm) distribution in rock samples 24
Figure 18: Contour map of Ba (ppm) distribution in rock samples 25
Figure 19: Contour map of Au (ppb) distribution in rock samples 26
Figure 20: Contour map of Fe (%) distribution in rock samples 27
Figure 21: Contour map of Pb (ppm) distribution in rock samples 28
Figure 22: Contour map of Mn (ppm) distribution in rock samples 30
Figure 23: Contour map of Zn (ppm) distribution in rock samples 31
Figure 24: Contour map of As (ppm) distribution in rock samples 32

TABLES

Table 1: Representative silicate whole rock and trace element analysis of quartz-phyric rhyolite (sample 71-90-05084), host rock to the Rod deposit 7
Table 2: Descriptive statistics, rock samples, Rod deposit area 9
Table 3: Matrix of Spearman nonparametric correlation coefficients, rock geochemical samples, Rod deposit area (N=30) 10
Table 4: Summary of statistically significant element pairs from Table 3. Pairs are grouped according to interpreted causal relationships 11

INTRODUCTION

The area overlying the Rod Cu-Zn massive sulphide deposit was selected for mercury vapour, humus, and rock geochemical surveys as part of mineral deposit programming under the Canada-Manitoba Mineral Development Agreement.

Anomalous concentrations of Cu, Zn, Co, Ni, Fe and Mn were discriminated among humus samples in proximity to the Rod deposit; conductivity and pH measurements were successful in duplicating the location and magnitude of trace metal anomalies. These methods possibly provide a tool for inexpensively pre-selecting target areas for trace metals that are significant in base metal exploration (Ferreira and Fedikow, 1988, 1990). Fedikow (1986) and Fedikow and Amor (1990) determined that the measurement of mercury vapour by Aurex cups yielded some anomalous, but non-correlatable, results for this survey area, and that the method is not reliable in indicating the presence of mercury vapour evolving from mercury-enriched mineral deposits (despite high contrast in Hg between bedrock and mineralization, i.e., 4200x at the Rod deposit).

Thirty rock samples were collected from the same sampling grid as the humus and mercury vapour samples and were analyzed for Mo, Cu, Pb, Zn, Ag, Ni, Co, Mn, Fe, As, U, Au, Th, Sr, Cd, Sb, Bi, V, Ca, P, La, Cr, Mg, Ba, Ti, B, Al, Na, K and W. Surface bedrock geology was mapped at a scale of 1:750 over the grid area. The analyses are reported and discussed in relation to surface bedrock geology, as well as the results of the aforementioned humus and mercury vapour surveys.

Ultimately, these data will be integrated with data from a regional rock geochemical survey of the Snow Lake area. The aim of the much larger study will be to delineate mineralization-related alteration and to provide a significant rock geochemical database for use in a spatial analysis study of geological data from the Snow Lake area.

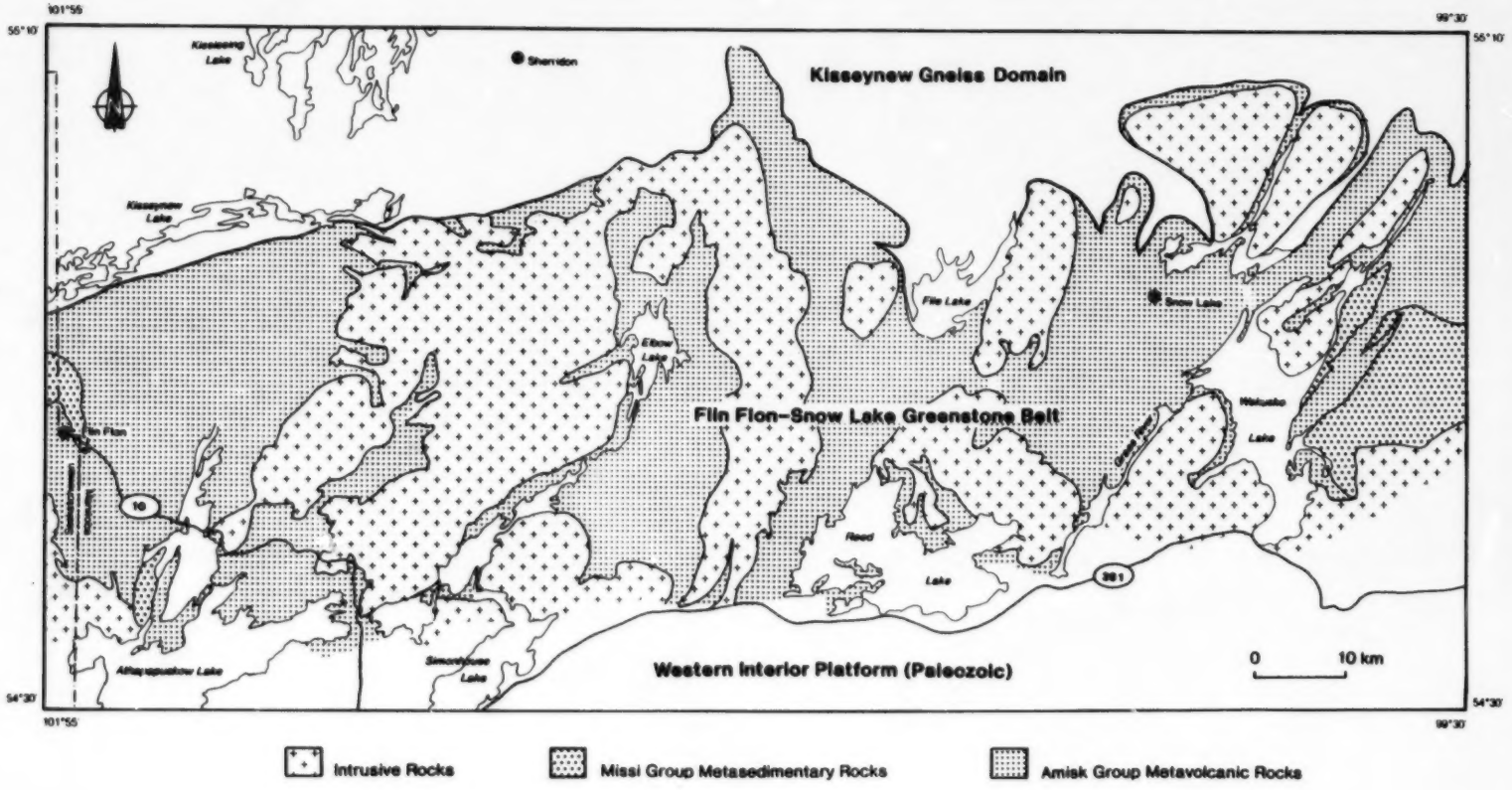

Figure 1: General geology of the Flin Flon-Snow Lake greenstone belt (after Bailes, 1971).

GEOLOGY

Regional Geology

The Flin Flon-Snow Lake greenstone belt comprises Proterozoic metamorphosed volcanic, sedimentary and intrusive rocks; it has a length of 250 km and an exposed width of 32 to 48 km (Fig. 1; Bailes *et al.*, 1987). The belt, part of the southern Churchill Province, is bound to the north by the Kisseynew sedimentary gneiss domain, and is overlain unconformably to the south by Ordovician dolomitic limestone.

Supracrustal rocks in the Flin Flon-Snow Lake greenstone belt may be subdivided into Amisk Group volcanic and associated sedimentary rocks and younger Missi Group epiclastic and minor volcanic rocks (Bruce, 1918). Amisk Group rocks, deposited primarily in subaqueous environments, consist of basaltic to rhyolitic volcanic and volcaniclastic rocks, and minor iron formation, conglomerate and other epiclastic rocks. Amisk Group rocks in the Snow Lake area include abundant felsic volcanic rocks, large areas of which have been hydrothermally altered, and volcanogenic greywacke turbidites (Bailes *et al.*, 1987). Missi Group rocks include sandstone and conglomerate interpreted as fluvial-alluvial deposits, and in the Snow Lake area, some subaerial and subaqueous volcanic rocks *(ibid.)*.

Multiple stages of deformation have affected rocks in the Snow Lake area, including an isoclinal folding event (F_1), a folding event that generated northeasterly trending axial traces (F_2), and the emplacement of gneiss domes (Froese and Moore, 1980). Major faults, including the McLeod Road Thrust Fault, and minor smaller fractures and shear zones are present. Rocks in the Snow Lake area have been metamorphosed to lower to upper amphibolite facies (Froese and Moore, 1980; Bailes *et al.*,1987).

Local Geology

Rod Deposit

The Rod Cu-Zn volcanogenic massive sulphide deposit occurs near the hinge of the Anderson Lake anticline, an isoclinal F_1 fold (Fig. 2; Gale and Koo, 1977), within the uppermost 100 m of the Lower Mine felsic unit, composed of intercalated mafic and felsic flows and pyroclastic rocks in the central part of the Amisk Group (Fig. 3; Bailes *et al.*,1987). Rocks enclosing the deposit include mafic flows and pyroclastic rocks, felsic pyroclastic rocks, and quartz porphyry. The mineralized zone, the hanging wall and, to a lesser extent, the footwall are carbonatized. A definitive study of alteration at the Rod deposit has not been undertaken. The Stall, Ram, Linda, and Anderson Cu-Zn deposits are interpreted to be situated in similar stratigraphic settings and structural environments (Froese and Moore, 1980).

The Rod deposit consists of two solid sulphide zones, the No. 1 and No. 2 Zones, that are enveloped by a zone of lower grade disseminated sulphide mineralization with an apparent width of 120 to 245 m. The average sulphide content in the solid sulphide zones is 40% chalcopyrite, 30% pyrite, 15% sphalerite, 12% pyrrhotite, 3% pyrite, and minor marcasite, galena, gold and silver (Coats *et al.*, 1970).

Stall Lake Mines Ltd. produced copper and zinc from the smaller No. 1 Zone from 1962 to 1964. Production from the No. 2 Zone commenced in 1984. It is owned by Falconbridge Ltd. (50%) and Stall Lake Mines Ltd. (50%) and is currently leased to Hudson Bay Mining & Smelting Co. Ltd. Production and reserves were estimated to total 688 000 tonnes of 7.2% Cu and 3.0% Zn (Esposito, 1986). This survey was conducted over the No. 2 Zone, and all further references to the Rod deposit will refer to the No. 2 Zone.

The No. 2 Zone strikes approximately northeast, dips 50° to 60°NW and plunges N25°E/25°-35°. The deposit is 533 m long in plan view, 46 to 61 m wide, and 3.65 m thick. The south end, top of the deposit, is 183 m below surface and the north end is 732 m below surface (Coats *et al.*, 1970).

Grid Area

The area sampled was mapped at a scale of 1:750 over two weeks in 1990 to provide a basic understanding of the bulk chemical composition of the rocks in the grid area (Fig. 4). A representative major and trace element analysis of quartz-phyric rhyolite, host to the Rod deposit, is presented in Table 1. Medium grained basalt with amphibole and feldspar porphyroblasts is exposed in the northernmost part of the map area. A unit of fine grained aphyric basalt, locally feldspar-phyric and fragmental, occurs to the south. Within these two basaltic lithologies are small areas of massive aphyric rhyolite, locally fragmental, garnetiferous and rusty weathered, and locally with an intrusive character. In the southwestern part of the map area near Stall Lake, the aphyric basalt is interlayered with quartz-phyric rhyolite. The southernmost and eastern parts of the area are also underlain by quartz-phyric rhyolite. Fine grained aphyric basalt, locally fragmental and feldspar-phyric, is interlayered with the rhyolite in places. Small mafic amphibole-feldspar-quartz dykes are present within the unit of quartz-phyric rhyolite. Foliations in the area are east- to northeast-striking.

A number of small, shallow, partially overgrown trenches are present in the southeastern part of the grid. The trenches expose boudinaged, discontinuous white quartz veins hosted by quartz-phyric rhyolite, which contain up to 5% (combined) galena, arsenopyrite, pyrite and chalcopyrite. The sulphide minerals occur as grains, blebs, pods and veinlets. Rhyolite is silicified adjacent to the veins.

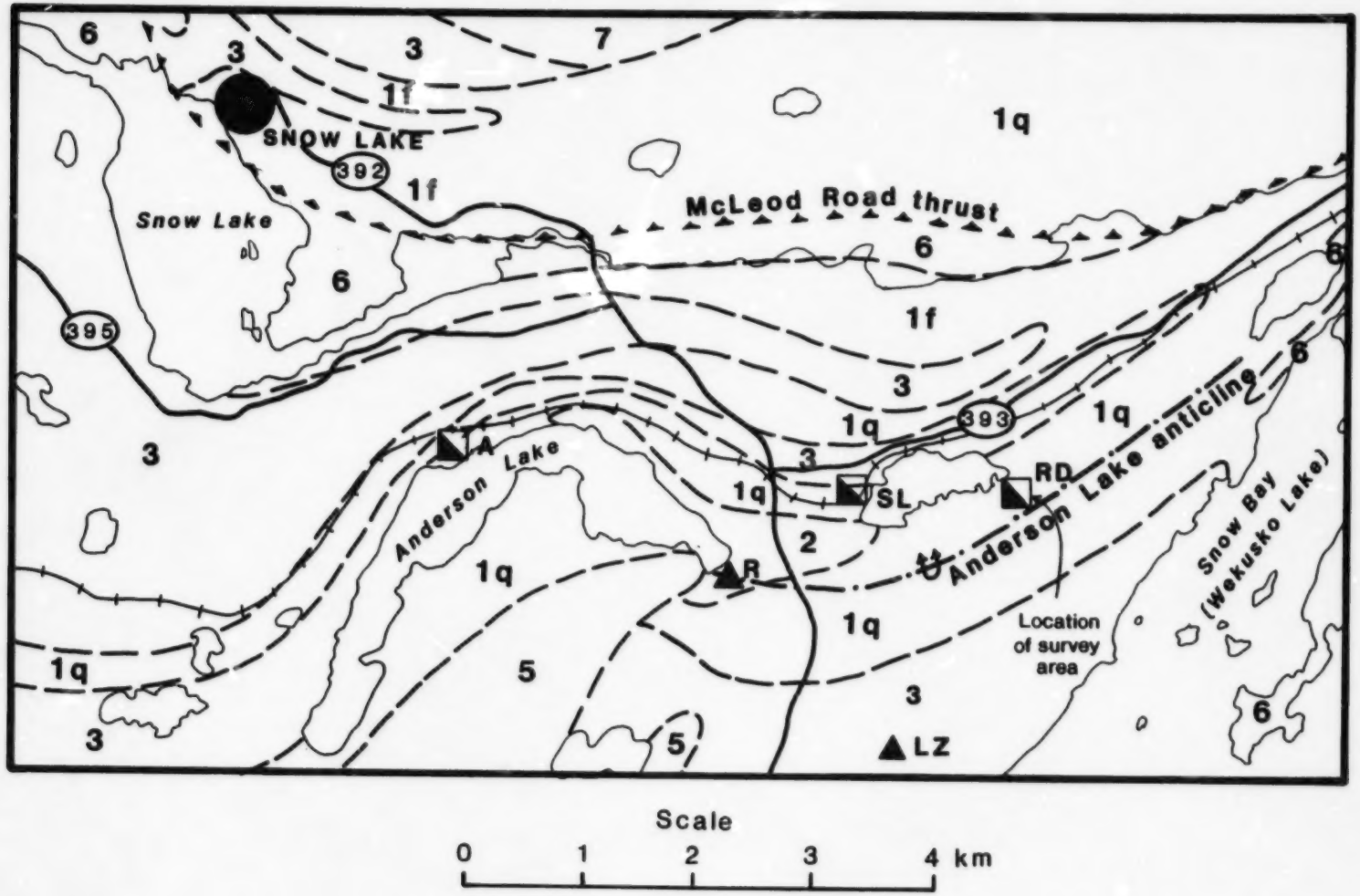

Figure 2: Geology of part of the Snow Lake area (after Froese and Moore, 1980). Amisk Group: 1 - Felsic pyroclastic and volcaniclastic rocks; q) quartz-eye; f) fragmental; 2 - Altered volcanic rocks of Unit 1; 3 - Mafic flows, pyroclastic and volcaniclastic rocks; 5 - Quartz-eye tonalite; 6 - Greywacke and shale. Missi Group: 7 - Lithic arenite. A - Anderson Lake Cu-Zn deposit; RD - Rod Lake Cu-Zn deposit; SL - Stall Lake Cu-Zn deposit; LZ - Linda Zone Cu-Zn deposit; R - Ram Zone Cu-Zn deposit.

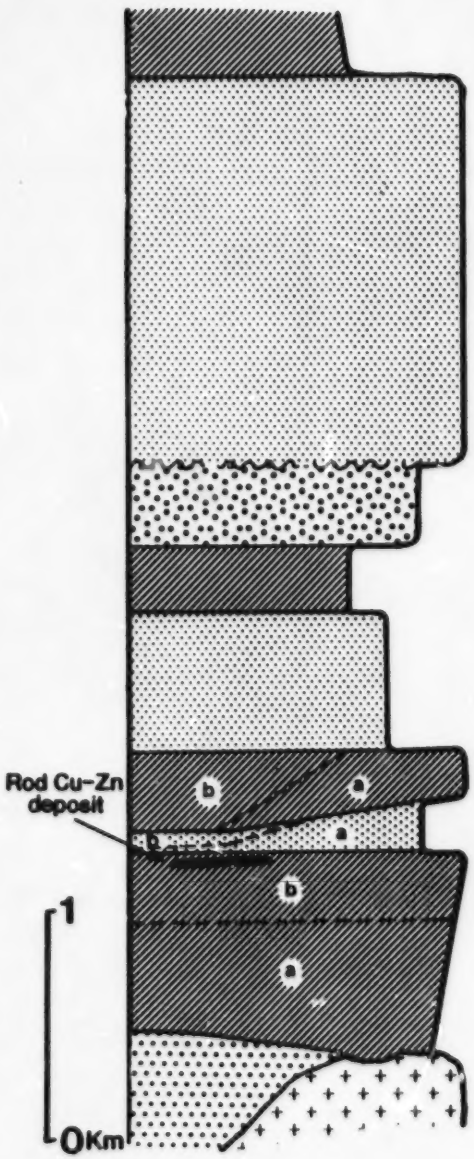

HERBLET, TOWNSITE AND SNOW CREEK BASALTS	
TOWNSITE RHYOLITE	With intercalated mafic volcanic rocks of overlying unit.
McLeod Road Thrust Fault	
GREYWACKE-MUDSTONE TURBIDITES	
MIXED VOLCANIC-SEDIMENTARY	Subequal amounts of felsic and mafic volcanic rocks, minor intercalated sediments.
THREEHOUSE BASALT	Plagioclase- and amphibole-phyric basalt flows, mafic epiclastic rocks.
HANGING WALL FELSIC	Discrete units of aphanitic (a) and coarsely porphyritic (b) rhyolite.
HANGING WALL MAFIC	Andesite (a) is pillowed near Stall Mine, epiclastic near Anderson Mine. Basalt (b) is similar to Threehouse basalt.
LOWER MINE FELSIC	Lower massive aphyric rhyolite (a) and upper predominantly fragmental rhyolite (b). Uppermost 100 m is quartz-phyric.
MAFIC FLOWS/BRECCIA	Aphyric mafic flows, mafic monolithologic and heterolithologic breccia.
SNEATH LAKE TONALITE	Probably subvolcanic.

Figure 3: Stratigraphic sequence in the Amisk Group, Anderson Lake area, showing setting of the Lower Mine felsic unit (after Bailes et al., 1987; nomenclature after Walford and Franklin, 1982).

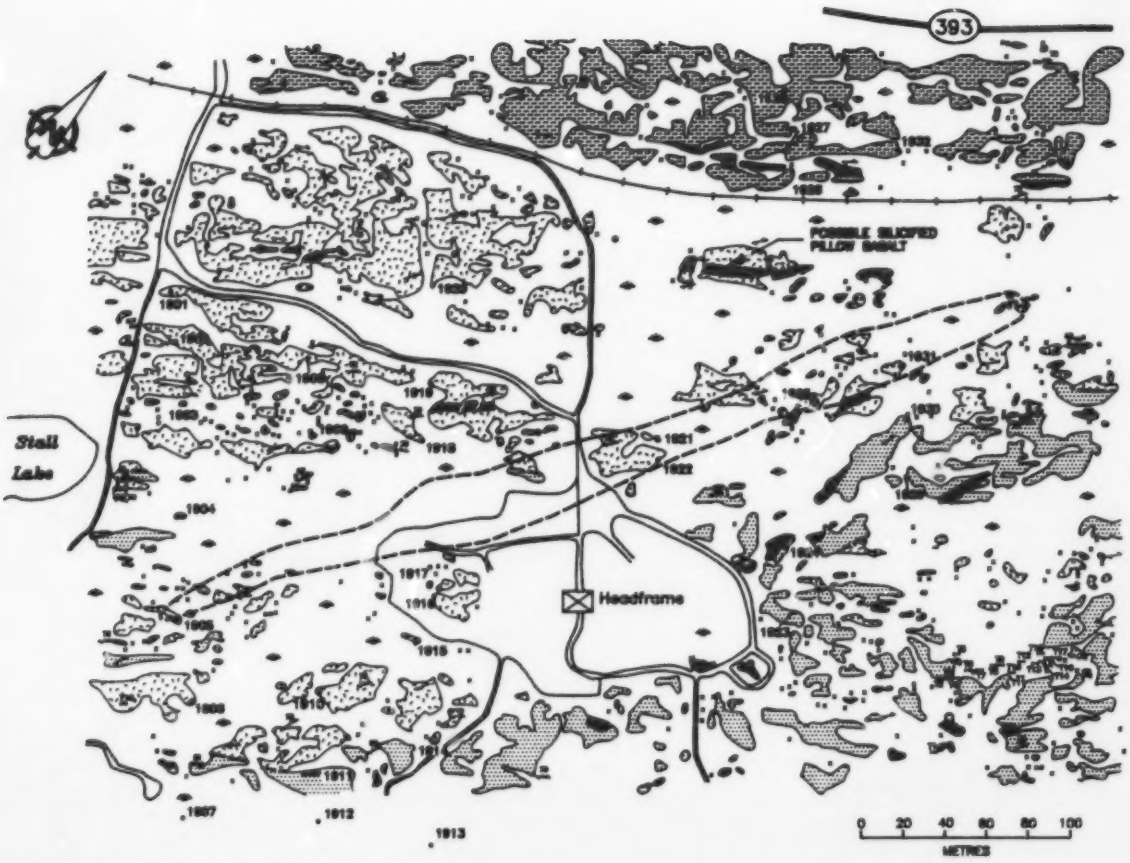

Figure 4: Geology in the area of the Rod Cu-Zn deposit.

Table 1: Representative silicate whole rock and trace element analysis of quartz-phyric rhyolite (sample 71-90-05084), host rock to the Rod deposit. The sample was collected southwest of the map area shown in Figure 4.

SiO_2	77.9 %
Al_2O_3	11.90
FeO	0.49
CaO	0.90
MgO	0.39
Na_2O	4.65
K_2O	1.93
TiO_2	0.24
P_2O_5	0.09
MnO	0.01
H_2O	0.37
S	0.01
CO_2	0.67
Other	0.03
Total	99.58

Ni	23 ppm
Cr	nd
Ba	131 ppm
Cu	28 ppm
Pb	nd
Zn	3 ppm
Mn	46 ppm

nd - not detected

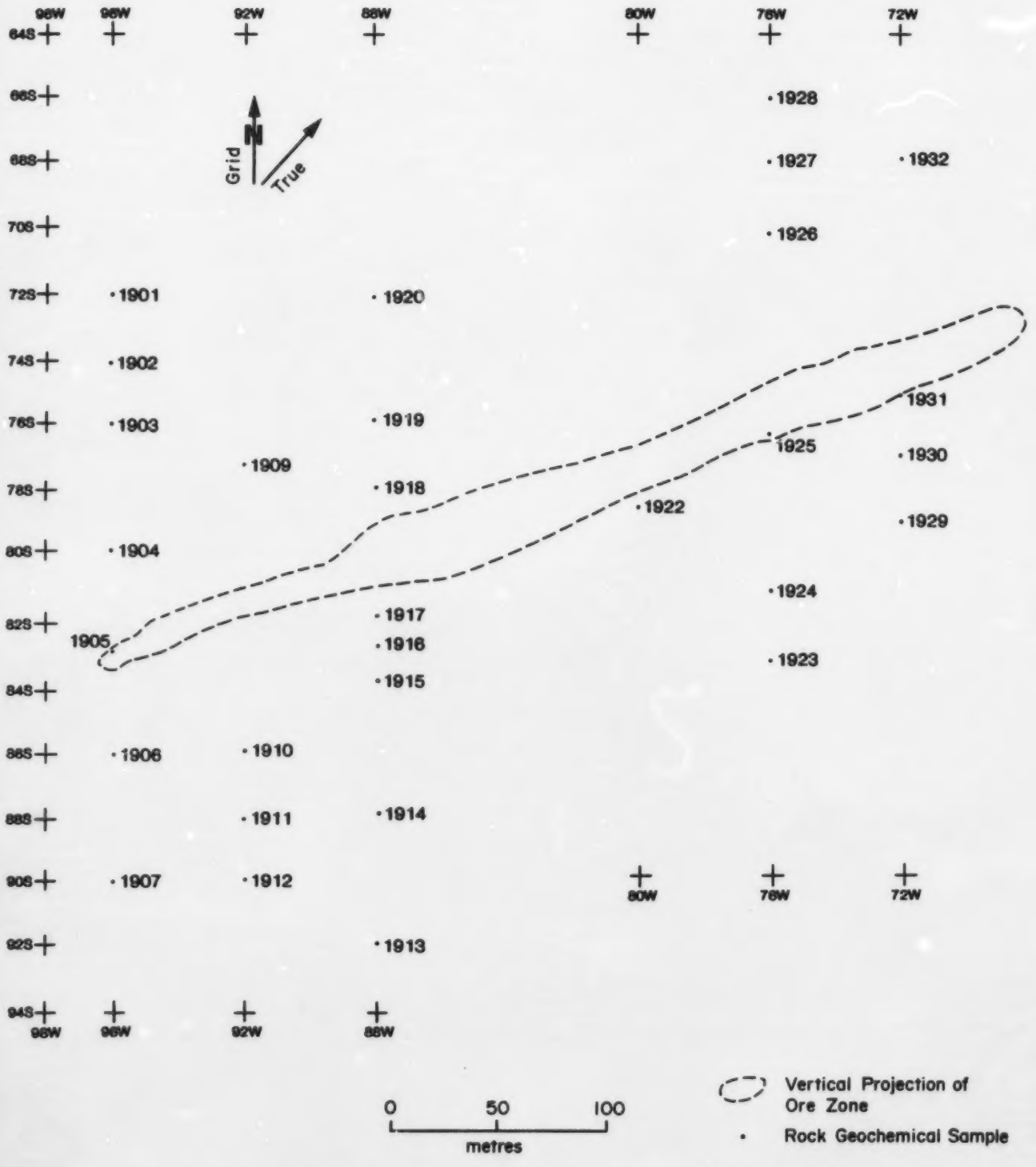

Figure 5: Grid map with sample numbers and locations.

SAMPLE COLLECTION, PREPARATION AND ANALYSIS

Thirty rock samples were collected in 1985 using a cut exploration grid for location control (Fig. 5)*. The locations of these samples were transferred to the geology map of the grid area (Fig. 4) following completion of field mapping in 1990. The surface infrastructure of the mine precluded complete sample coverage. Samples were collected as representative rock chips from available outcrop to give approximately 1 kg of sample for analysis.

Rock chips were jaw crushed to 0.5 cm diameter, then pulverized with a Braun pulverizer. A 0.500 g homogenized representative split sample was digested in 3 ml HCl-HNO_3-H_2O (3:1:2) at 95°C for one hour and diluted to 10 ml with deionized water**. The samples were analyzed for Mo, Cu, Pb, Zn, Ag, Ni, Co, Mn, Fe, As, U, Au, Th, Sr, Cd, Sb, Bi, V, Ca, P, La, Cr, Mg, Ba, Ti, B, Al, Na, K, and W by inductively coupled plasma atomic absorption spectrophotometry. Analyses were conducted by Acme Analytical Laboratories, Vancouver. Analytical reproducibility is better than 17% for all elements above the detection limit.

Results

Analytical results are presented in Appendix I; histograms of data for individual elements are presented in Appendix II. Analyses for Mo, Ag, U, Th, Cd, Sb, Bi, La, Cr, Ti and W were either below the analytical limits of detection or else have ranges that are too small to discriminate anomalies; no further consideration is given to these elements.

Descriptive statistics for the remaining elements are given in Table 2. Data distributions that are highly skewed and peaked, as measured by skewness and kurtosis statistics, indicate the presence of multiple populations within the dataset, i.e., background or low concentrations, and anomalous or high concentrations. The data for these elements may be arbitrarily divided into three groups: (1) elements with low skewness and kurtosis statistics (i.e., both skewness and kurtosis $\leq \pm 2.00$), viz., Cu, Ni, Co, Sr, V, Ca, P, Mg, B, Al, Na and K); (2) elements with moderate skewness or kurtosis statistics (either skewness or kurtosis $\pm 2.00 < x < \pm 10.00$, viz., Zn, Mn, Fe, Ba, Au and Pb); and (3) elements with high skewness or kurtosis statistics (i.e., either skewness or kurtosis $\geq \pm 10.00$, viz., As).

Table 2: Descriptive statistics, rock samples, Rod deposit area

Element	Arithmetic Mean (x)	Median	Mode	Minimum Value	Maximum Value	Standard Deviation	Variance	Skewness	Kurtosis	Threshold
Al, %	2.38	2.08	3.23	0.65	6.08	1.34	1.81	1.14	1.06	2.8
As, ppm	5	3	2	2	22	4	16	3.03	12.06	8
Au, ppb	7	3	1	1	38	8	73	2.24	5.61	8
B, ppm	10	10	2	2	22	5	30	0.56	-0.07	12
Ba, ppm	131	107	3	3	554	125	15656	2.01	4.20	152
Ca, %	2.08	1.81	0.55	0.31	5.90	1.42	2.01	1.07	1.01	3
Co, ppm	10	10	11	4	20	4	13	0.72	1.18	13
Cu, ppm	105	101	77	26	197	46	2121	0.36	-0.47	110
Fe, %	3.51	3.43	2.83	1.44	7.76	1.13	1.27	1.73	6.25	3.66
K, %	0.36	0.31	0.08	0.01	0.97	0.27	0.07	0.83	-0.17	0.36
Mg, %	0.86	0.83	0.77	0.34	1.81	0.31	0.10	0.71	1.64	1.27
Mn, ppm	407	395	395	202	812	120	14356	1.34	3.69	530
Na, %	0.26	0.24	0.09	0.07	0.68	0.17	0.03	0.76	-0.38	0.1
Ni, ppm	9	9	9	4	13	2	5	-0.47	-0.04	5
P, %	0.037	0.035	0.012	0.012	0.065	0.016	0.000	0.27	-1.05	0.037
Pb, ppm	4	4	3	2	13	2	5	2.10	6.08	7
Sr, ppm	46	25	7	2	166	50	2529	1.30	0.59	10
V, ppm	72	74	15	6	206	47	2193	0.91	1.26	22
Zn, ppm	48	44	34	18	129	24	574	1.51	3.18	28

* Directions given in this text are made with respect to grid orientation, i.e., 'north' refers to grid north, not true north.

** This leach is partial for Mn, Fe, Ca, P, Cr, Mg, Ba, Ti, B, Al, Na, K and W.

Table 3: Matrix of Spearman nonparametric correlation coefficients, rock geochemical samples, Rod deposit area (N=30)

	Cu	Pb	Zn	Ni	Co	Mn	Fe	As	Sr	V	Ca	P	Mg	Ba	B	Al	Na	K	Au
Cu	1.00																		
Pb	0.21	1.00																	
Zn	-0.08	0.19	1.00																
Ni	0.24	0.13	-0.18	1.00															
Co	0.54*	0.21	0.19	0.32	1.00														
Mn	0.13	0.24	0.71*	-0.03	0.54*	1.00													
Fe	0.20	0.22	0.69*	-0.05	0.66*	0.73*	1.00												
As	-0.35	-0.02	-0.06	0.18	-0.27	-0.07	-0.13	1.00											
Sr	0.19	0.24	-0.31	0.11	-0.00	-0.17	-0.30	-0.23	1.00										
V	0.51*	0.19	-0.13	0.45*	0.89*	0.35	0.37	-0.24	0.22	1.00									
Ca	0.41	0.42	-0.28	0.34	0.14	0.02	-0.20	0.04	0.78*	0.35	1.00								
P	0.20	0.14	0.24	0.01	0.37	0.16	0.32	-0.54*	0.36	0.29	0.16	1.00							
Mg	0.40	0.20	0.22	0.20	0.80*	0.54*	0.48*	-0.44*	0.26	0.74*	0.25	0.46*	1.00						
Ba	-0.25	0.04	0.57*	0.02	0.27	0.47*	0.39	-0.38	-0.10	0.10	-0.24	0.46*	0.39	1.00					
B	-0.09	0.06	-0.24	0.12	-0.19	-0.19	-0.39	-0.04	0.78*	-0.01	0.59*	0.03	0.04	-0.06	1.00				
Al	0.25	0.38	-0.16	0.14	0.14	0.09	-0.08	-0.05	0.81*	0.31	0.88*	0.18	0.34	-0.10	0.69*	1.00			
Na	0.31	0.30	-0.35	0.19	0.17	-0.05	-0.23	-0.16	0.86*	0.42	0.88*	0.31	0.39	-0.11	0.62*	0.90*	1.00		
K	-0.35	0.03	0.79*	-0.23	0.22	0.64*	0.67*	-0.13	-0.39	-0.09	-0.45	0.29	0.29	0.78*	-0.33	-0.27	-0.38	1.00	
Au	0.45*	0.15	-0.03	0.45*	0.51*	0.18	0.20	0.01	-0.08	0.53*	0.15	0.03	0.29	-0.04	-0.18	-0.07	0.04	-0.09	1.00

* - *denotes statistical significance at the 99% level of confidence*

High standard deviations and variances, measures of dispersion within the dataset, indicate data distributions that are not normal. Datasets that have both background and anomalous populations produce large dispersion statistics. Elements from Group 1 have mostly low to moderate standard deviations, except for Sr, which has high dispersion statistics. Elements from Group 2 have low to high standard deviations. Arsenic, the only element in Group 3, has moderately high dispersion statistics.

A Spearman nonparametric correlation coefficient matrix is presented in Table 3. A nonparametric correlation coefficient matrix was used because visual examination of histograms and tabled dispersion statistics indicates that the data distributions for the elements of interest are not normal, and more closely approximates lognormality. Elements from Group 1 are omitted from the matrix because their data distributions are characterized by low dispersion statistics. This feature suggests the absence of multiple populations in the dataset. Strontium, identified as a member of Group 1, is included in the matrix because of its high standard deviation relative to other elements in Group 1. Variable pairs for which a significant linear relationship exists at a 99% level of confidence are marked with an asterisk.

Thirty-five pairs of statistically significant elements are present in the matrix. These pairs are summarized in Table 4, where they are grouped into relevant categories. Pairs listed under 'Lithology' are representative of the relationships between elements in rock-forming minerals in the lithologies sampled. The 'Mineralization' pairs are indicative of the sulphide minerals that characterize the Rod deposit and its related alteration (i.e., Cu, Zn, Ni, Co, Fe, Au). The Cu and Zn are present in chalcopyrite and sphalerite, and the Ni, Co and Fe are present in pyrrhotite and pyrite, and possibly nickeliferous pentlandite. Au is correlated with Co, Ni and Cu, a definite sulphide association. The correlation between Zn and Ba and K is interesting and suggests either (i) potassic metasomatism with corresponding introduction of Zn, or (ii) sphalerite-barite-mica alteration. It is noteworthy that Ba is correlated with K (potassic metasomatism?), whereas P is correlated with Ba (a primary exhalite characteristic). The Sr-Ca association reflects carbonatization (Coats *et al.*, 1970). The negative correlations of As-P and As-Mg simply may reflect the arsenopyrite-bearing mineralizing process in quartz-phyric rhyolite in the southeast area of the grid.

Table 4: Summary of statistically significant element pairs from Table 3. Pairs are grouped according to interpreted causal relationships

Lithology	Mineralization	Alteration
Ca-B	Cu-Co	Sr-Ca (carbonatization)
Ca-Al	Cu-V	P-Ba
Ca-Na	Cu-Au	Ba-K (potassic metasomatism)
Ca-K	Zn-Mn	As-P (negative correlation)
P-Mg	Zn-Fe	As-Mg (negative correlation)
Fe-Mg	Zn-Ba	
Fe-K	Zn-K	
Sr-Al	Ni-V	
Sr-Na	Ni-Au	
V-Mg	Co-Mn	
Sr-B	Co-Fe	
Mn-Fe	Co-V	
Mn-Mg	Co-Mg	
Mn-Ba	Co-Au	
Mn-K		
B-Al		
B-Na		
Al-Na		

Contour diagrams are used to show the variation in placement and magnitude of values for individual elements. The threshold values between background and anomalous populations were determined graphically by the method of Tennant and White (1959), and are summarized in Table 2. Several data populations within a dataset may lead to threshold determinations that are not discriminating or may inaccurately reflect the data distribution (Fedikow, 1986; Fedikow and Ferreira, 1987); therefore, threshold values were adjusted and contour intervals were selected upon visual inspection of the dataset. Anomalous results above the threshold values are shaded in contour diagrams.

GROUP 1 - Low Skewness and Kurtosis ($\leq \pm 2.00$)

Elements with skewness and kurtosis statistics $\leq \pm 2.00$ include Al, B, Ca, Co, Cu, Na, Ni, K, Mg, P, Sr and V. Inflections indicating separate data populations on the cumulative frequency curves for these elements are poorly defined. These observations reflect elements whose datasets contain low-contrast, poorly defined anomalies.

Aluminum (Fig. 6)

Three broad areas of high Al concentrations are present: (1) a three-sample anomaly on the western side of the grid (40 x 125 m; 3.23-4.27% Al); (2) a single-sample anomaly at 83S/88W (3.39% Al); and (3) a comparatively high-contrast anomaly in the northeastern part of the grid (70 x 80 m; 3.86-6.08% Al).

Boron (Fig. 7)

A low-contrast three-sample B anomaly is present in the northeastern corner of the grid (up to 120 x 50 m; 15-22 ppm B). Two single-sample B anomalies are also present: (1) 80S/96W; 17 ppm B; (2) 86S/96W; 19 ppm B.

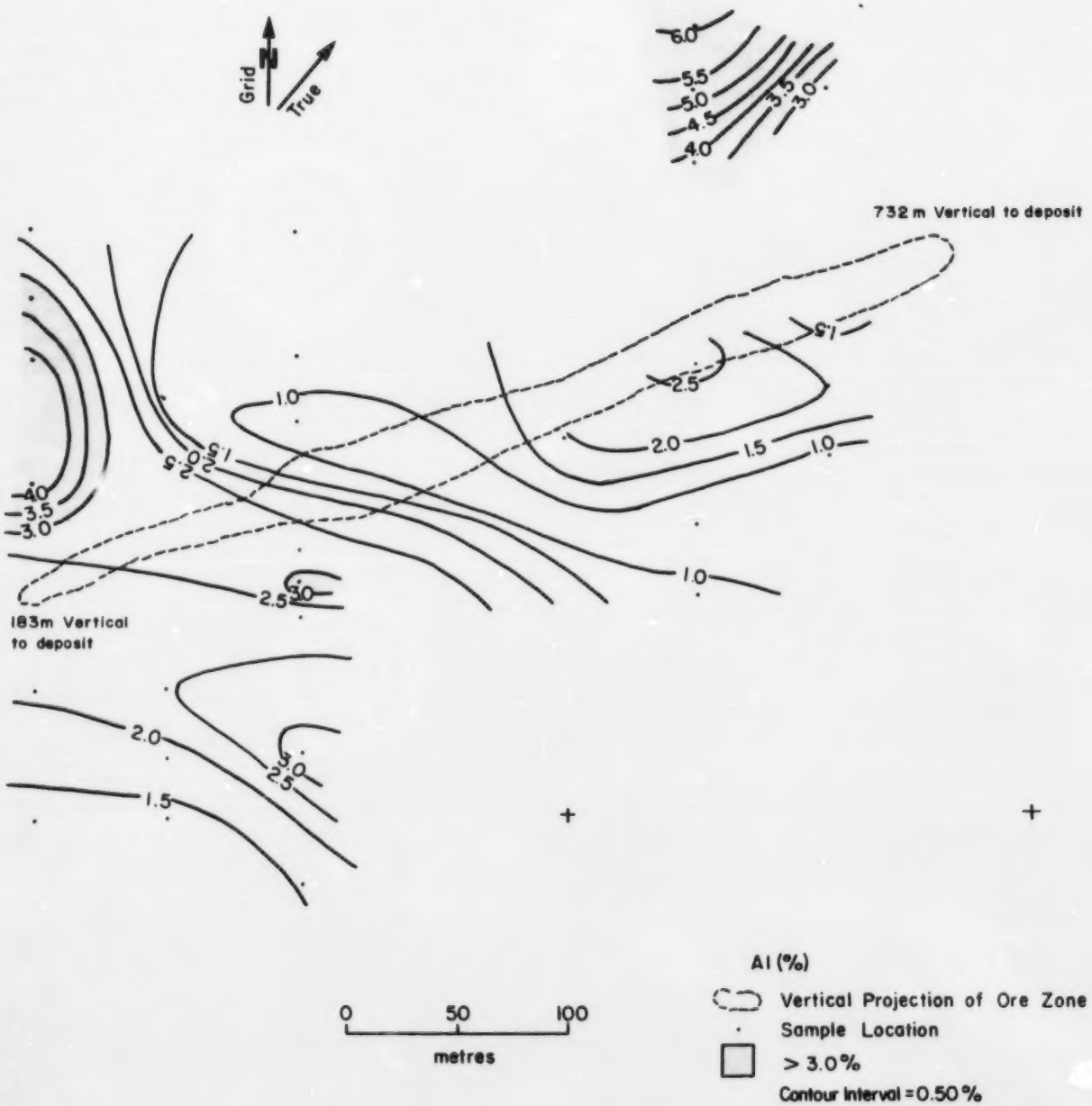

Figure 6: Contour map of Al (%) distribution in rock samples.

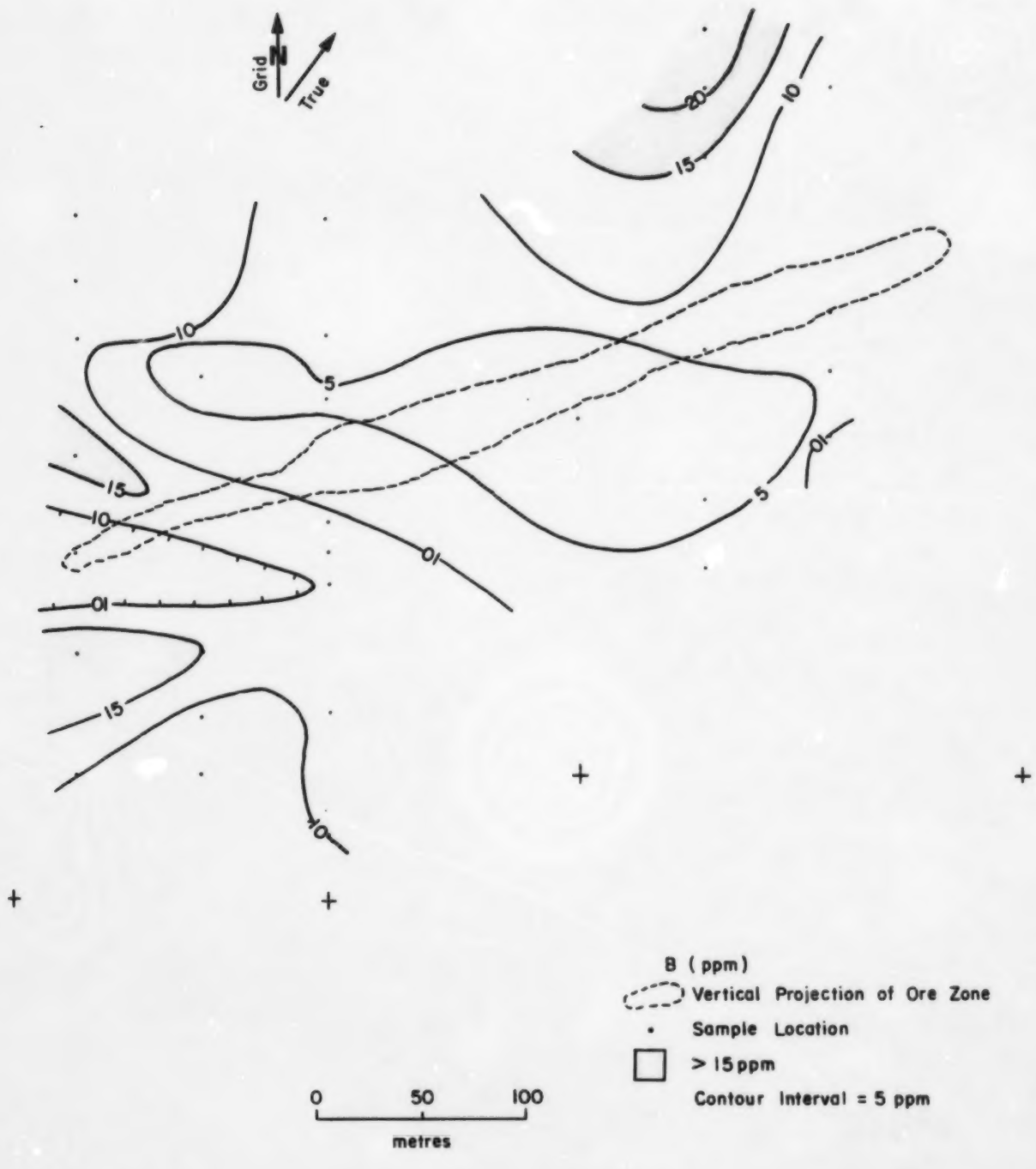

Figure 7: Contour map of B (ppm) distribution in rock samples.

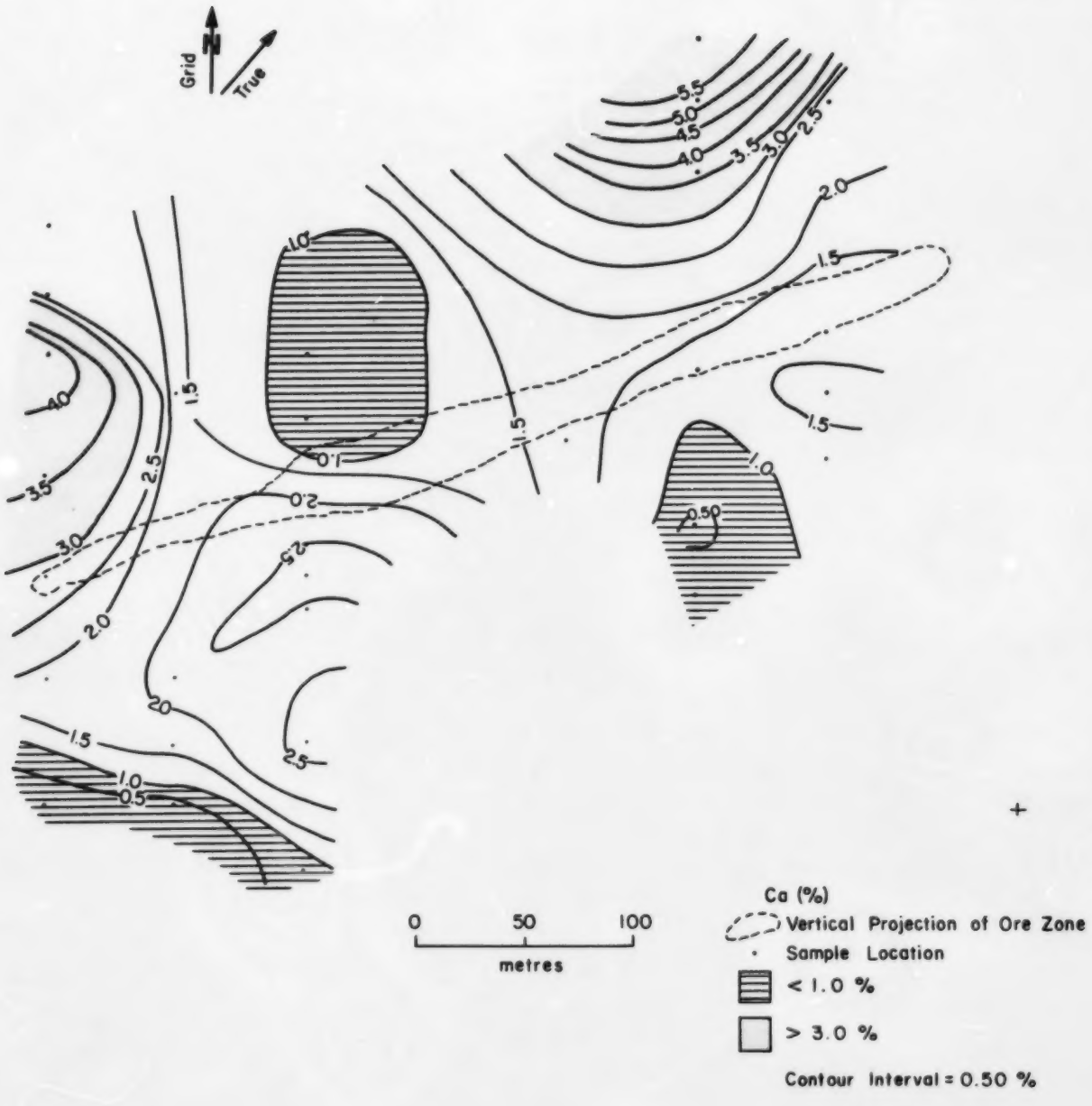

Figure 8: Contour map of Ca (%) distribution in rock samples.

Calcium (Fig. 8)

Two areas have very high Ca concentrations: (1) a three-sample anomaly along 76W in the northeastern part of the grid (up to 160 x 90 m; 3.68-5.90% Ca), and (2) a two-sample anomaly at 76S/96W - 80S/96W (3.65-4.20% Ca). Three areas have very low Ca concentrations: (1) three samples in the southwestern part of the grid (91S/92-96W; 0.31-0.83% Ca); (2) two samples in the southeastern part of the grid along 76S (0.48, 0.55% Ca); and (3) two samples along 88W (0.55, 0.80% Ca).

Cobalt (Fig. 9)

The maximum value for Co from this dataset is 20 ppm, which may be considered low for rock geochemical analyses in general. However, based on the distribution for this dataset, two single-sample anomalies are defined: (1) 76S/96W, 17 ppm; and (2) 83S/96W, 20 ppm.

Copper (Fig. 10)

A broad bifurcating high Cu zone covers most of the area of the grid (up to 350 x 110 m; 131-197 ppm Cu). In addition, a sample at 72S/88W contained 152 ppm Cu. The maximum value of Cu for this dataset is 195 ppm, with a mean of 105 ppm, which is not notably elevated despite the proximity of significant Cu mineralization (i.e., No. 1 Zone to the west and No. 2 Zone at depth).

Magnesium (Fig. 11)

Two single-sample Mg anomalies are present: (1) 83S/96W; 1.81% Mg, and (2) 76S/76W; 1.26% Mg.

Nickel (Fig. 12)

A two-sample low-contrast anomaly is present in the southeastern part of the grid (80S/72W, 12 ppm Ni; 82S/76W, 13 ppm Ni). Five low-contrast single-sample anomalies are present: (1) 76S/96W, 12 ppm; (2) 83S/96W, 13 ppm; (3) 78S/88W, 11 ppm; (4) 66S/76W, 11 ppm; and (5) 70S/76W, 11 ppm. The maximum value for Ni is 13 ppm, which is low.

Phosphorus (Fig. 13)

A broad low-contrast P anomaly is present over the southwestern part of the grid (up to 150 x 200 m; 0.050-0.065% P). Two low-contrast single-sample anomalies are defined: (1) 78S/72W (0.041% P), and (2) 66S/76W (0.046% P).

Potassium (Fig. 14)

Three areas of very high K contents are defined: (1) a band, up to 350 x 100 m, across the central part of the grid (0.54-0.75% K); (2) the southwestern portion of the grid (88-90S/88-96W; 0.61-0.97% K); and (3) a single-sample anomaly at 84S/76W (0.57% K). Two areas of anomalously low K concentrations are defined: (1) a band across the northern part of the grid up to 300 x 50 m (0.05-0.08% K); and (2) a single-sample anomaly at 78S/88W (0.01% K).

Sodium (Fig. 15)

The sharply defined threshold value for Na (0.10% Na) discriminates anomalies of Na depletion: (1) a two-sample anomaly at 76-78S/88W (0.08-0.09% Na); (2) a two-sample anomaly at 91S/92-96W (0.09, 0.09% Na); (3) a two-sample anomaly at 80-82S/72-76W (0.07, 0.09% Na); and (4) a single-sample anomaly at 76S/72W (0.07% Na).

Strontium (Fig. 16)

Strontium is exceptional within this group because of its high standard deviation (σ=50; x=46). Anomalously high Sr values occur: (1) in a band, 175 x 15 m, in the western part of the grid (146-166 ppm Sr); (2) at 88S/88W (164 ppm Sr); and (3) at 70S/76W (125 ppm Sr). Anomalously low Sr values occur: (1) in the west-central part of the grid (170 x 50 m; 2-5 ppm Sr); (2) in the southeast part of the grid (130 x 70 m; 5-8 ppm Sr); and (3) at 90S/92W (7 ppm Sr).

Vanadium (Fig. 17)

Three single-sample sites have very high V concentrations: (1) 76S/96W (133 ppm V); (2) 83S/96W (206 ppm V); and (3) 78S/88W (171 ppm V). Two broad areas with very low V concentrations are defined: (1) in the northwestern part of the grid (190 x 80 m; 6-15 ppm V); and (2) in the southeastern part of the grid (50 x 100 m; 15-21 ppm V).

GROUP 2 - Moderate Skewness or Kurtosis
($\pm$ 2.00 < x < $\pm$ 10.00)

Elements with moderate skewness or kurtosis statistics, i.e., either skewness or kurtosis $\pm$ 2.00 < x < $\pm$ 10.00, include Ba, Au, Fe, Pb, Mn, and Zn.

Barium (Fig. 18)

Three anomalies are defined in the southern part of the grid: (1) 88-92S/88-96W (up to 180 x 70 m; 111-427 ppm Ba); (2) a broadly extrapolated two-sample anomaly along 84S (up to 260 x 60 m; 166, 202 ppm Ba); and (3) 83S/96W (554 ppm; single sample).

Gold (Fig. 19)

The maximum value for Au from this dataset is 38 ppb. A broad bilobate area up to 140 x 200 m in the western part of the grid contains 12-38 ppb Au.

Iron (Fig. 20)

Two anomalous areas are defined: (1) a band approximately 385 x (15-65) m across the lateral centre of the grid (4.22-4.86% Fe), and (2) a single-sample anomaly at 83S/96W (7.76% Fe).

Lead (Fig. 21)

Only one sample point, 74S/96W, is anomalous (13 ppm Pb).

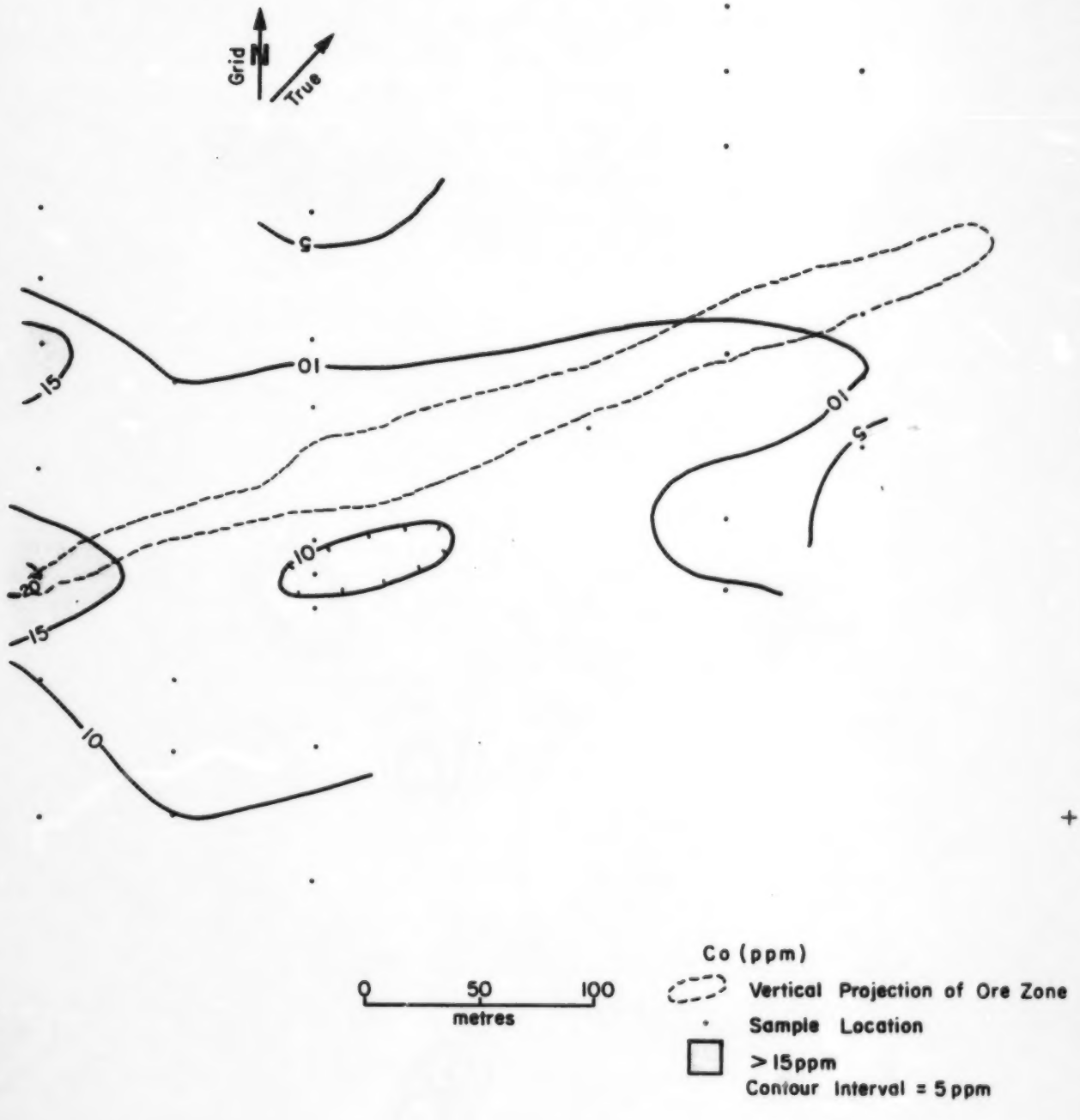

Figure 9: Contour map of Co (ppm) distribution in rock samples.

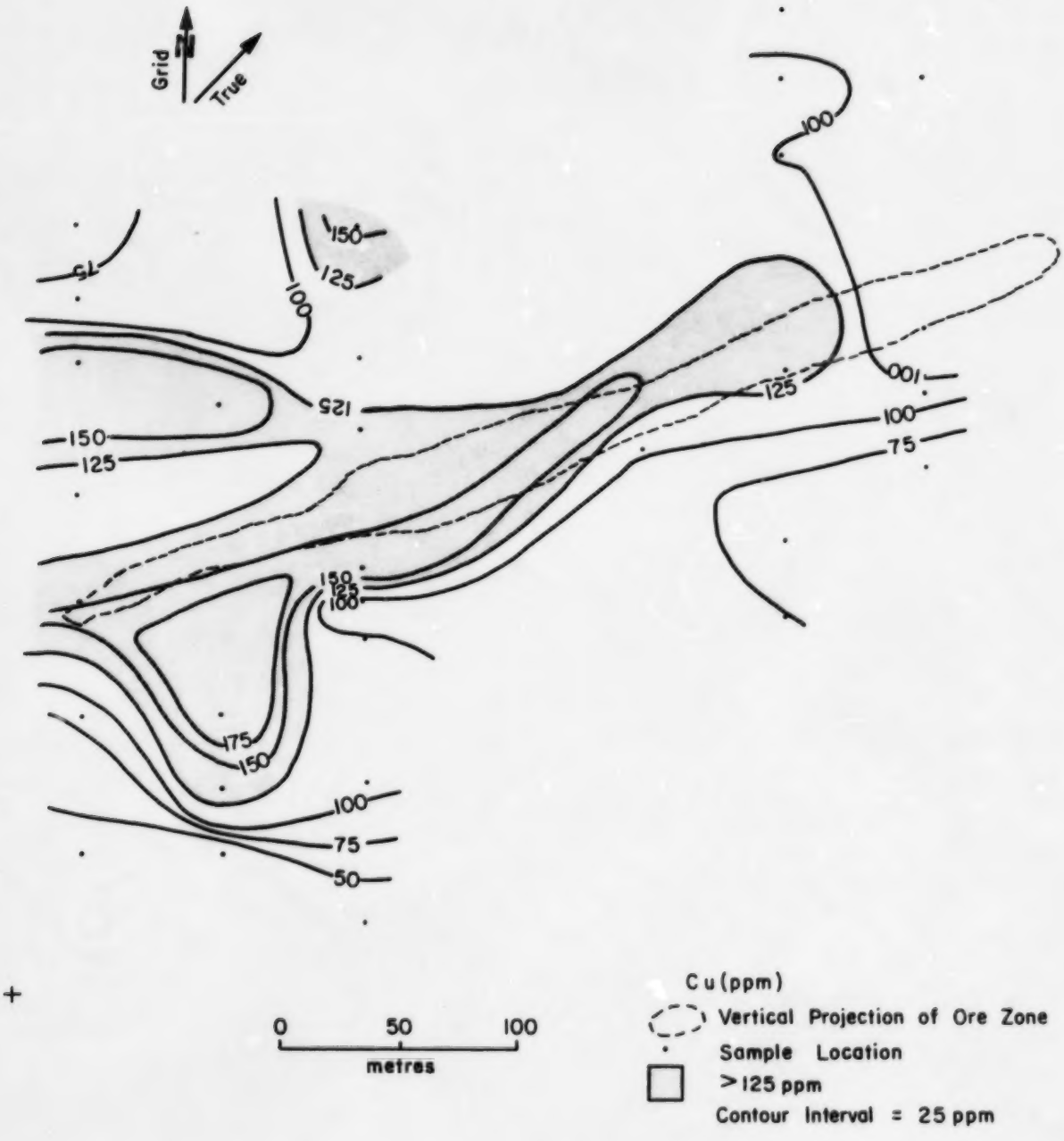

Figure 10: Contour map of Cu (ppm) distribution in rock samples.

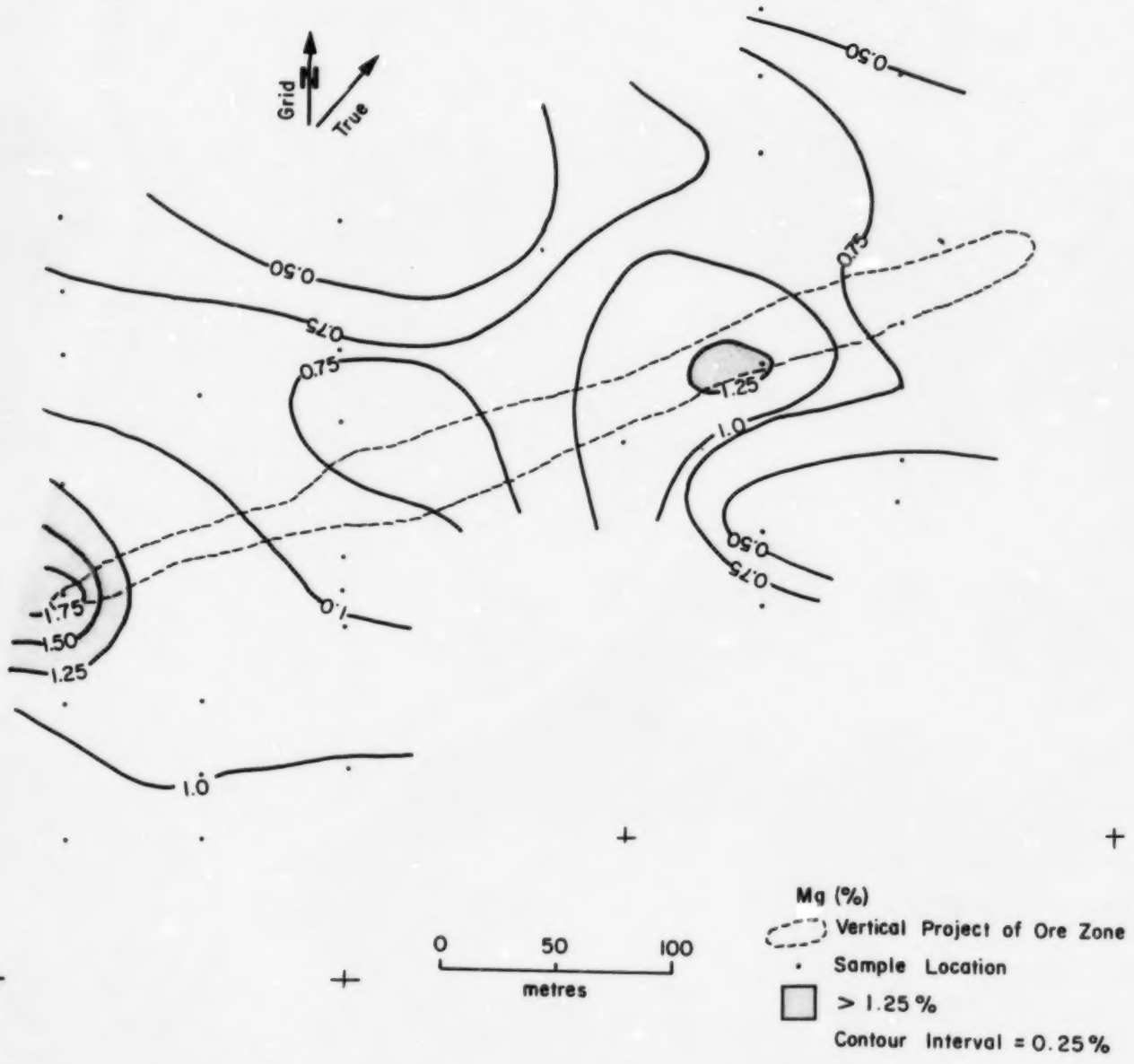

Figure 11: Contour map of Mg (%) distribution in rock samples.

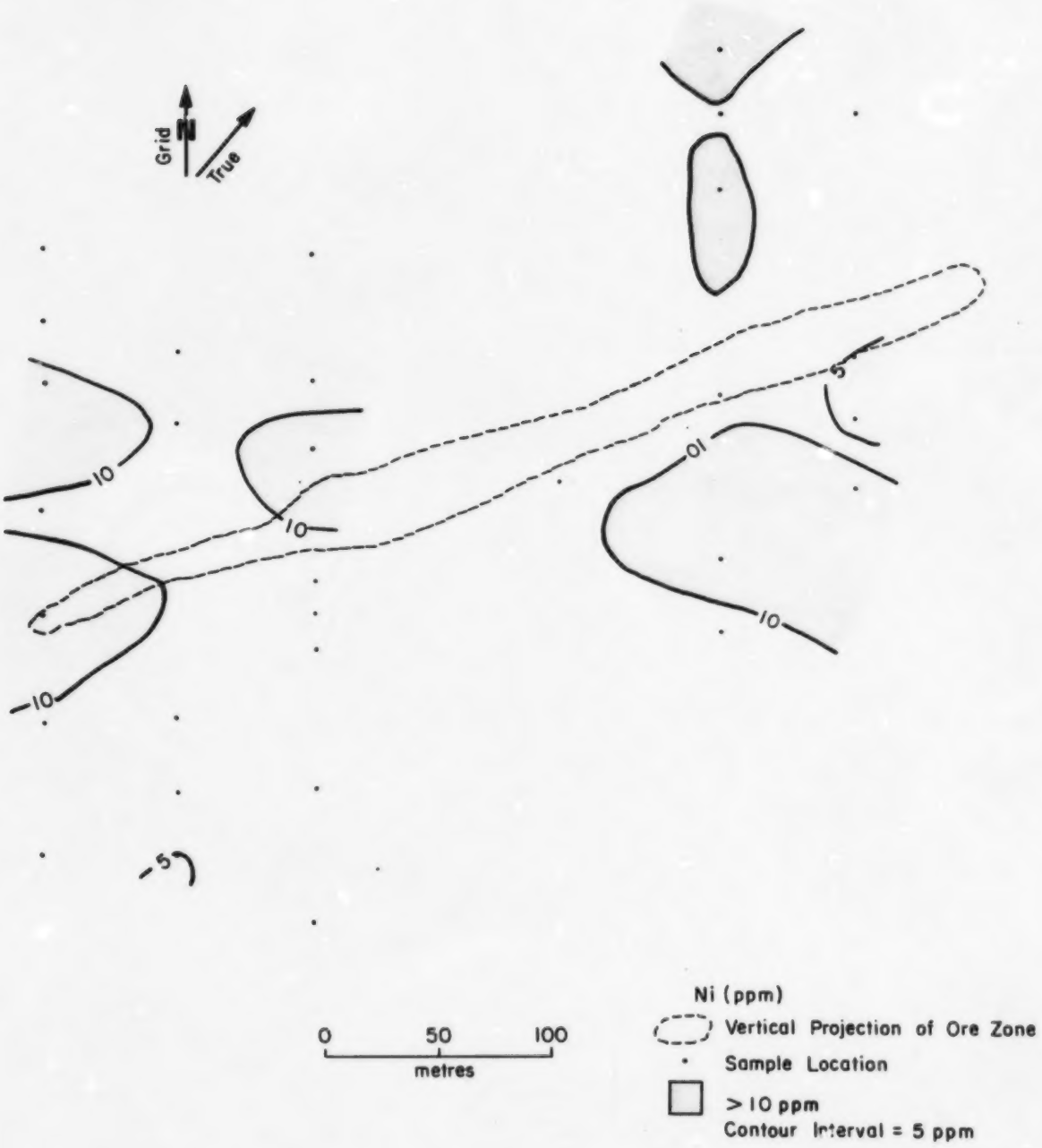

Figure 12: Contour map of Ni (ppm) distribution in rock samples.

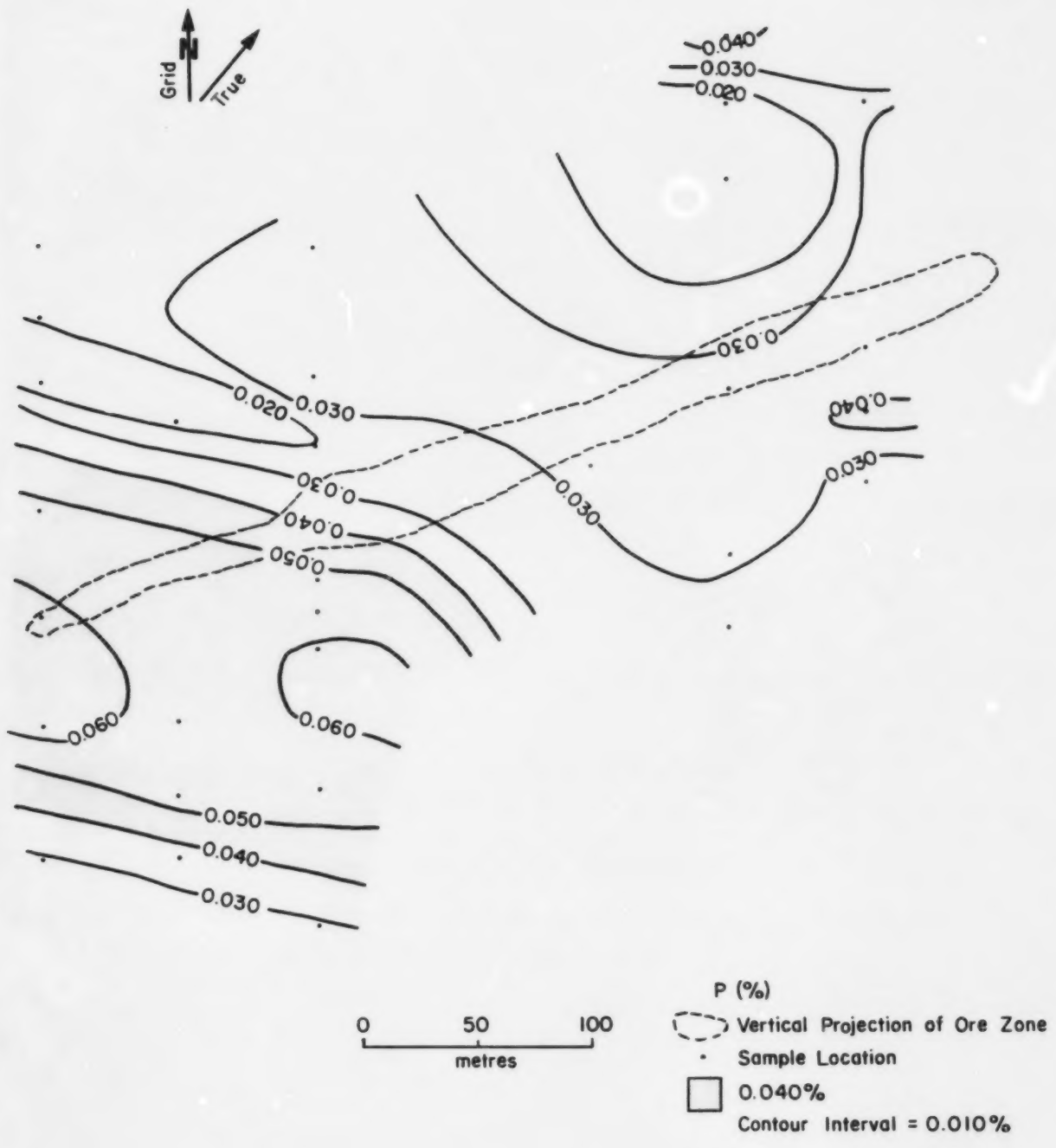

Figure 13: Contour map of P (%) distribution in rock samples.

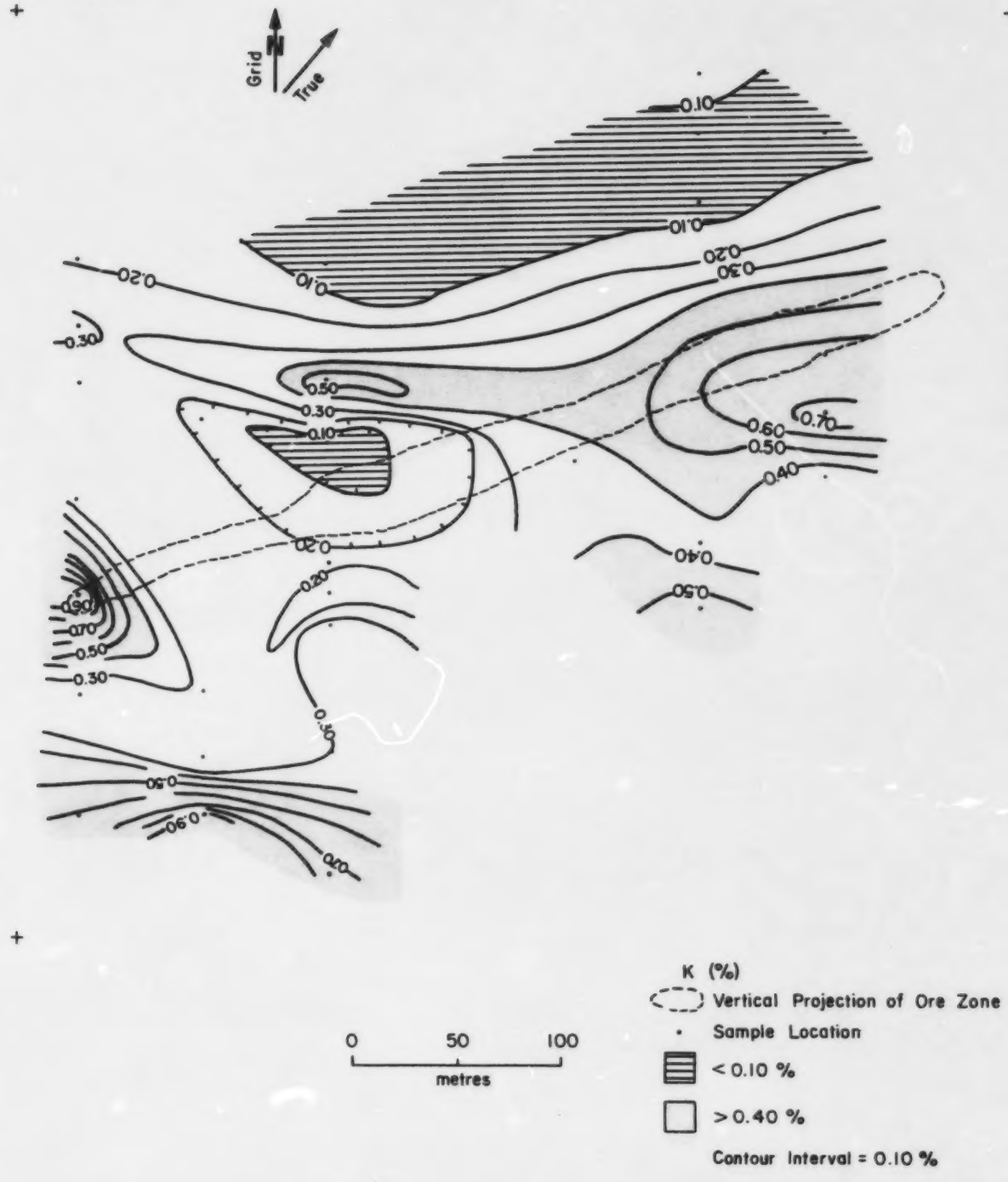

Figure 14: Contour map of K (%) distribution in rock samples.

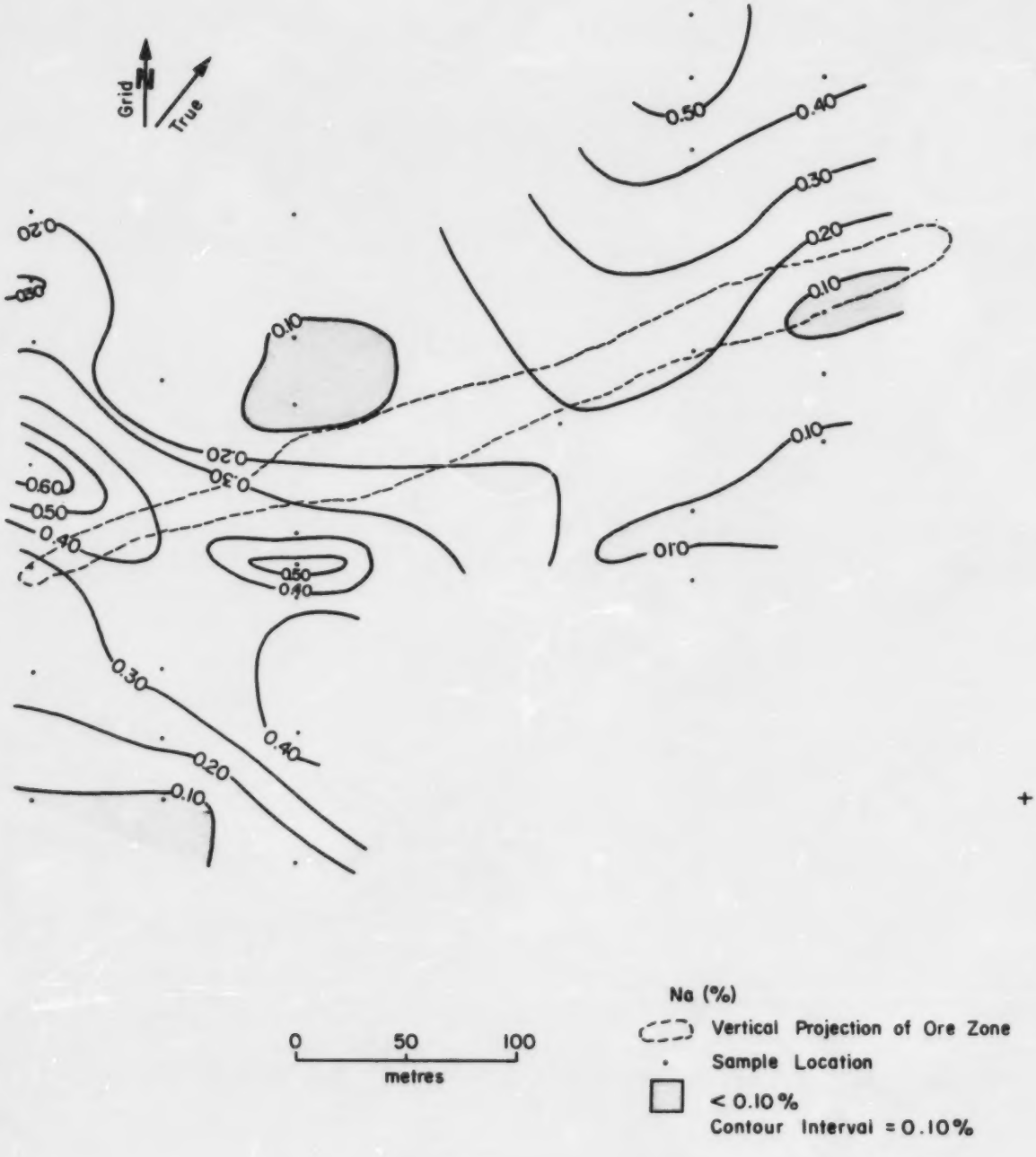

Figure 15: Contour map of Na (%) distribution in rock samples.

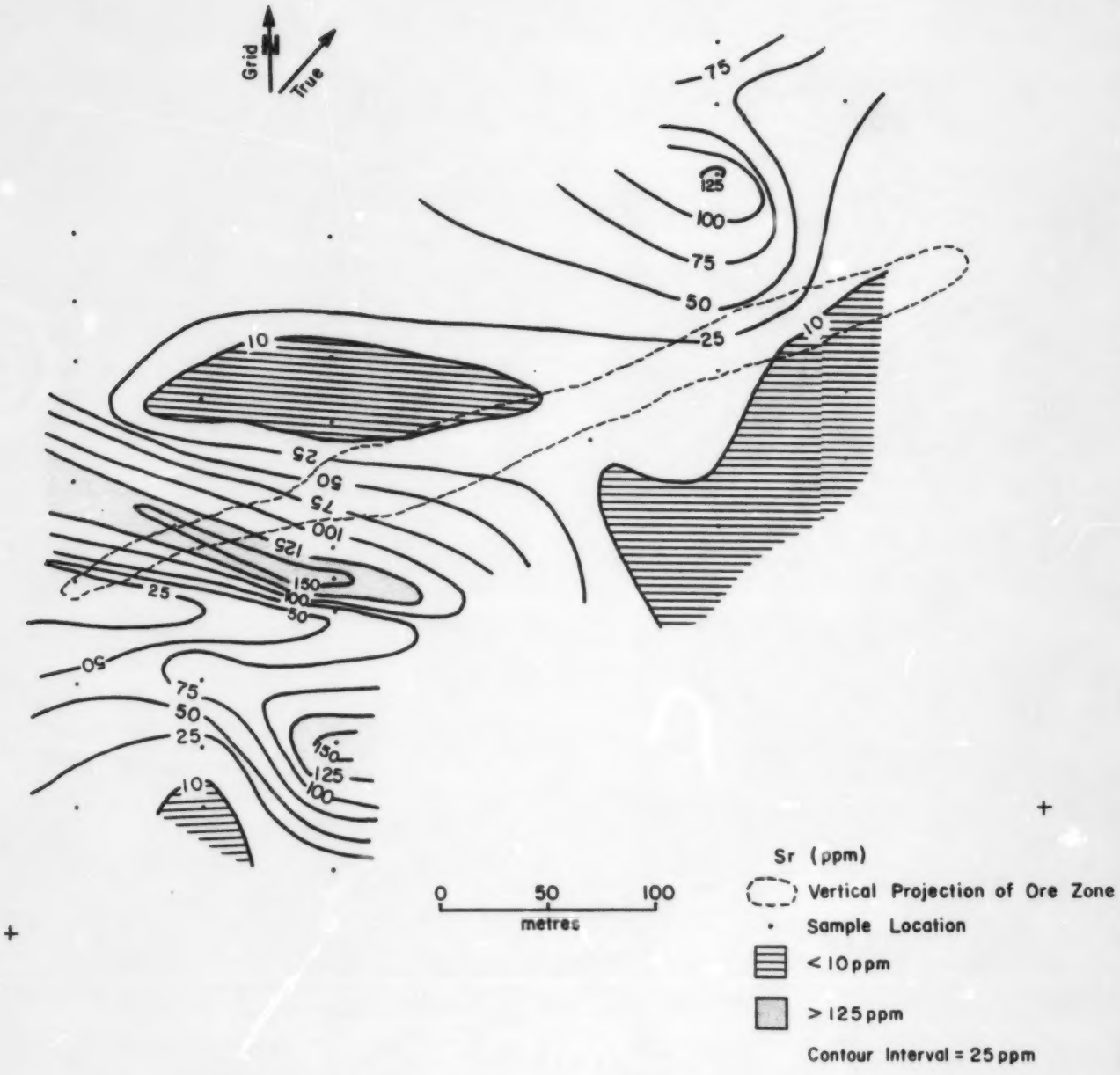

Figure 16: Contour map of Sr (ppm) distribution in rock samples. An extra contour, at 10 ppm, has been added to delineate areas of anomalously low (i.e., < 10 ppm Sr) concentrations.

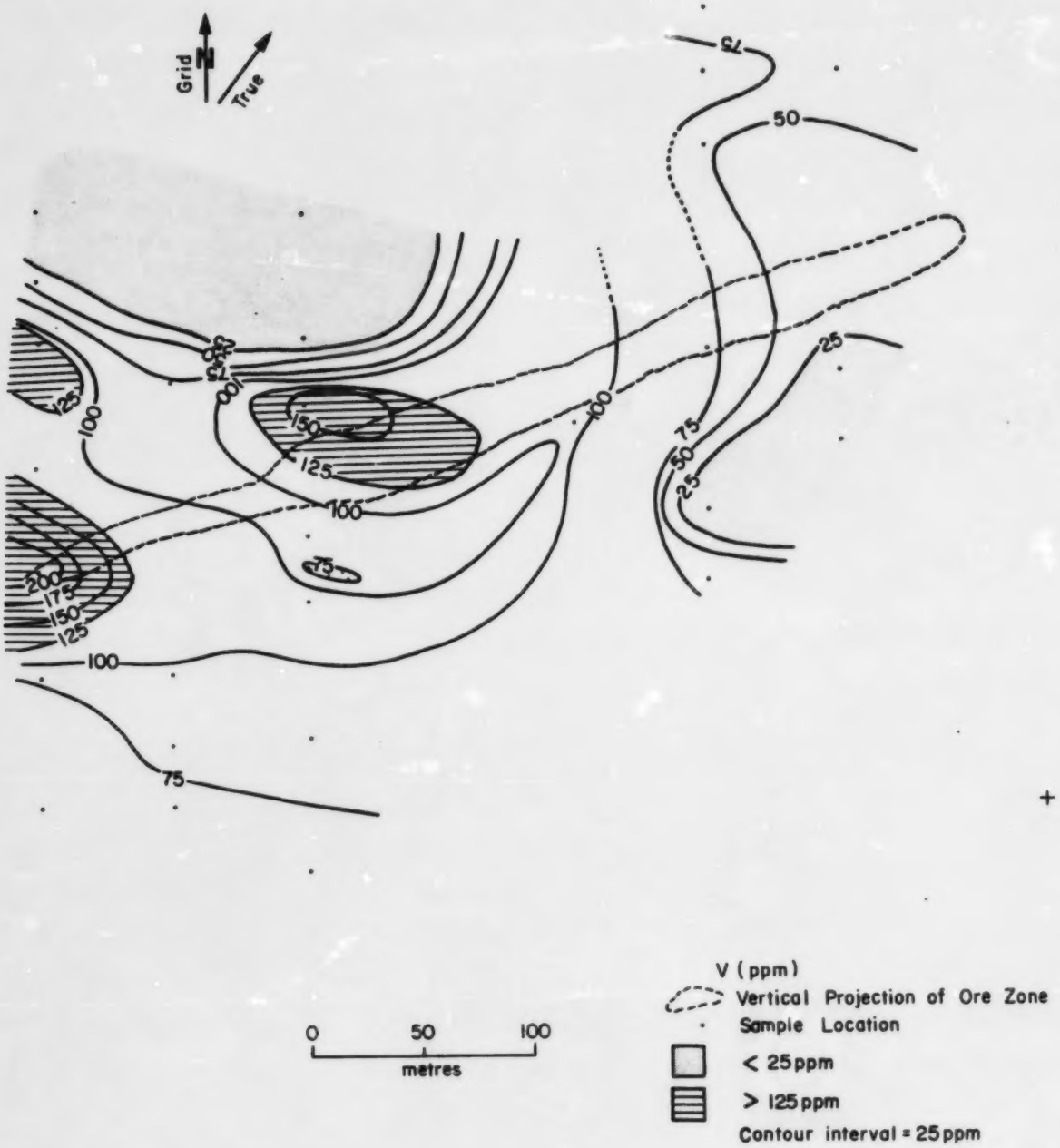

Figure 17: Contour map of V (ppm) distribution in rock samples.

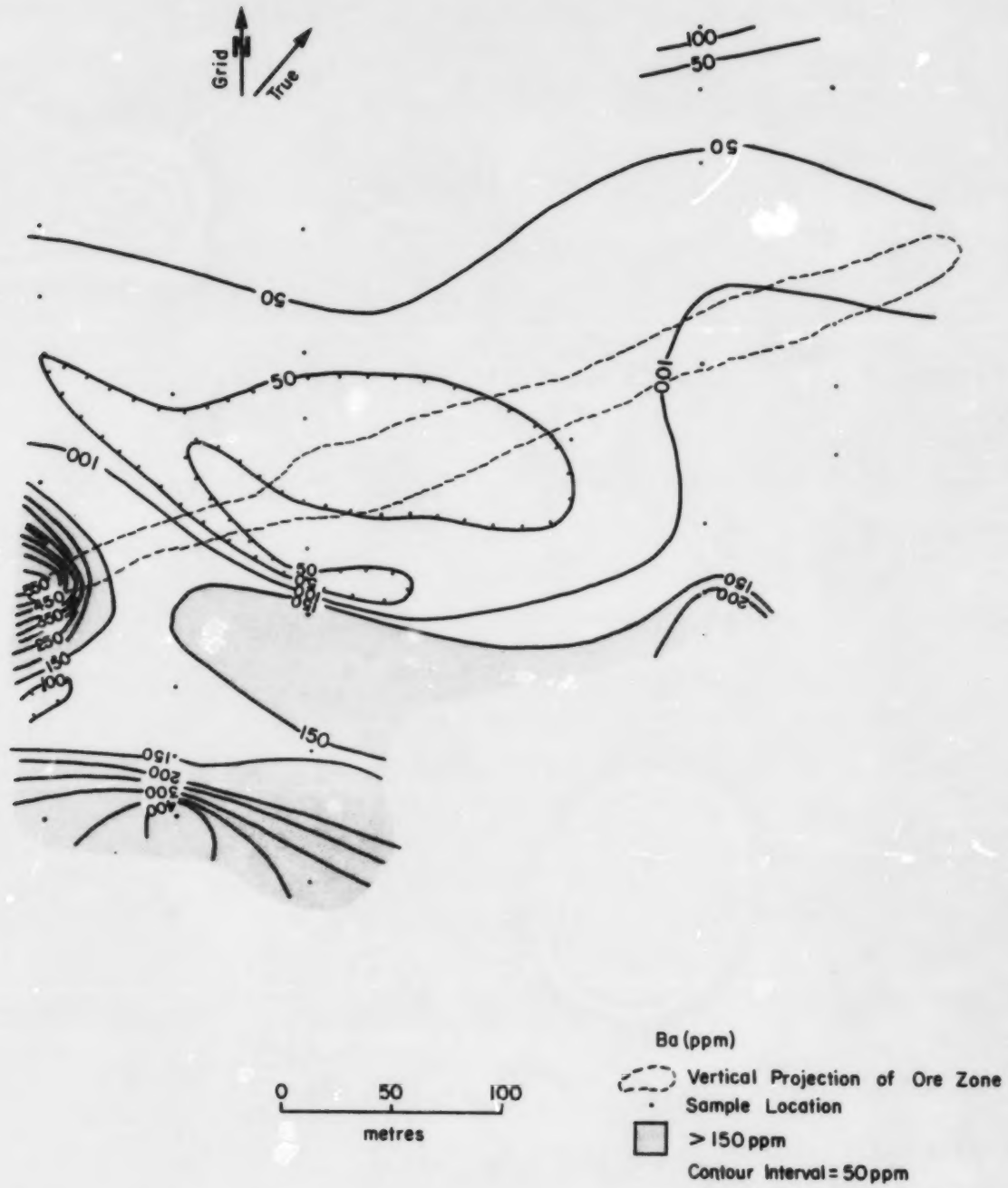

Figure 18: Contour map of Ba (ppm) distribution in rock samples.

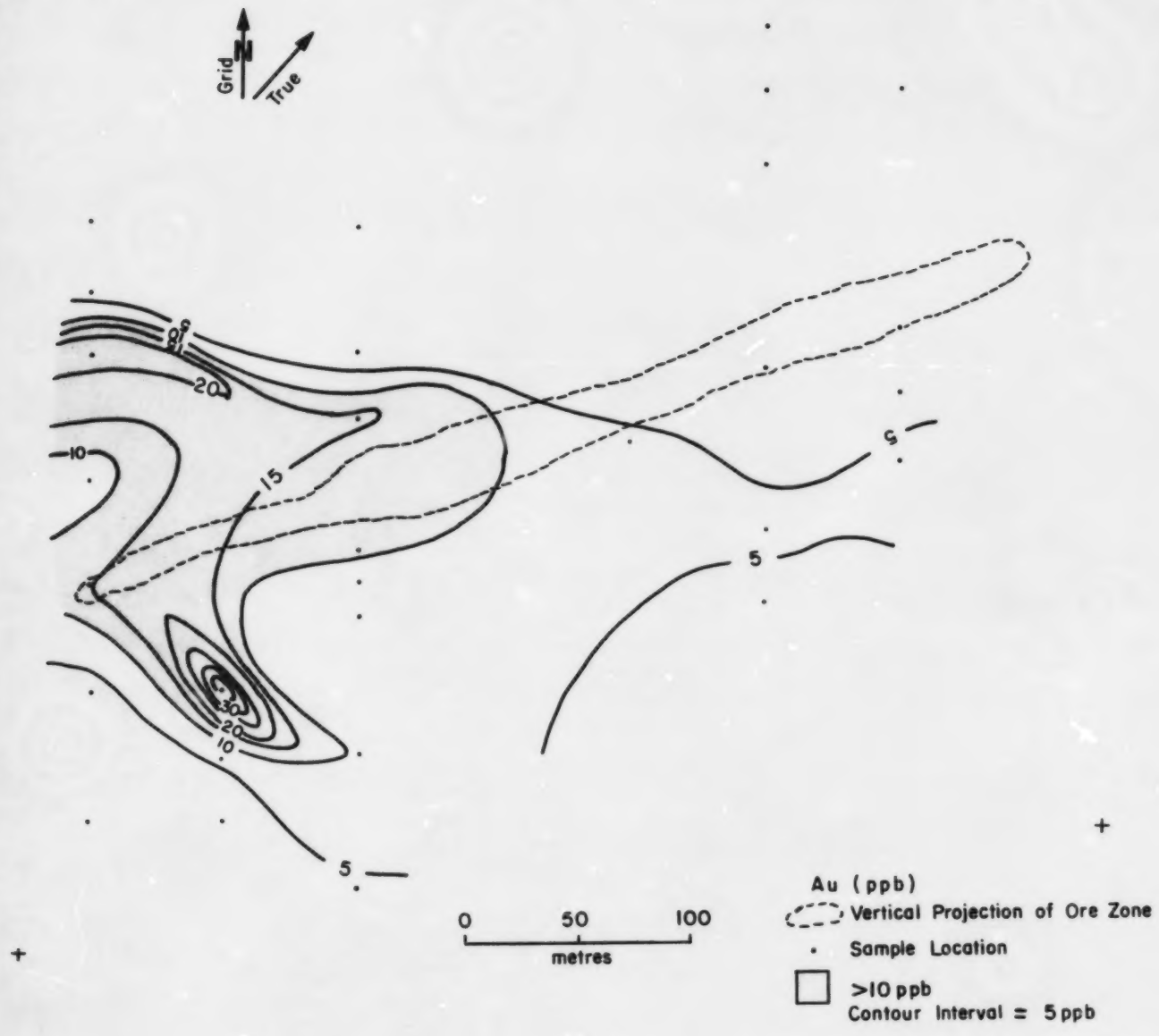

Figure 19: Contour map of Au (ppb) distribution in rock samples.

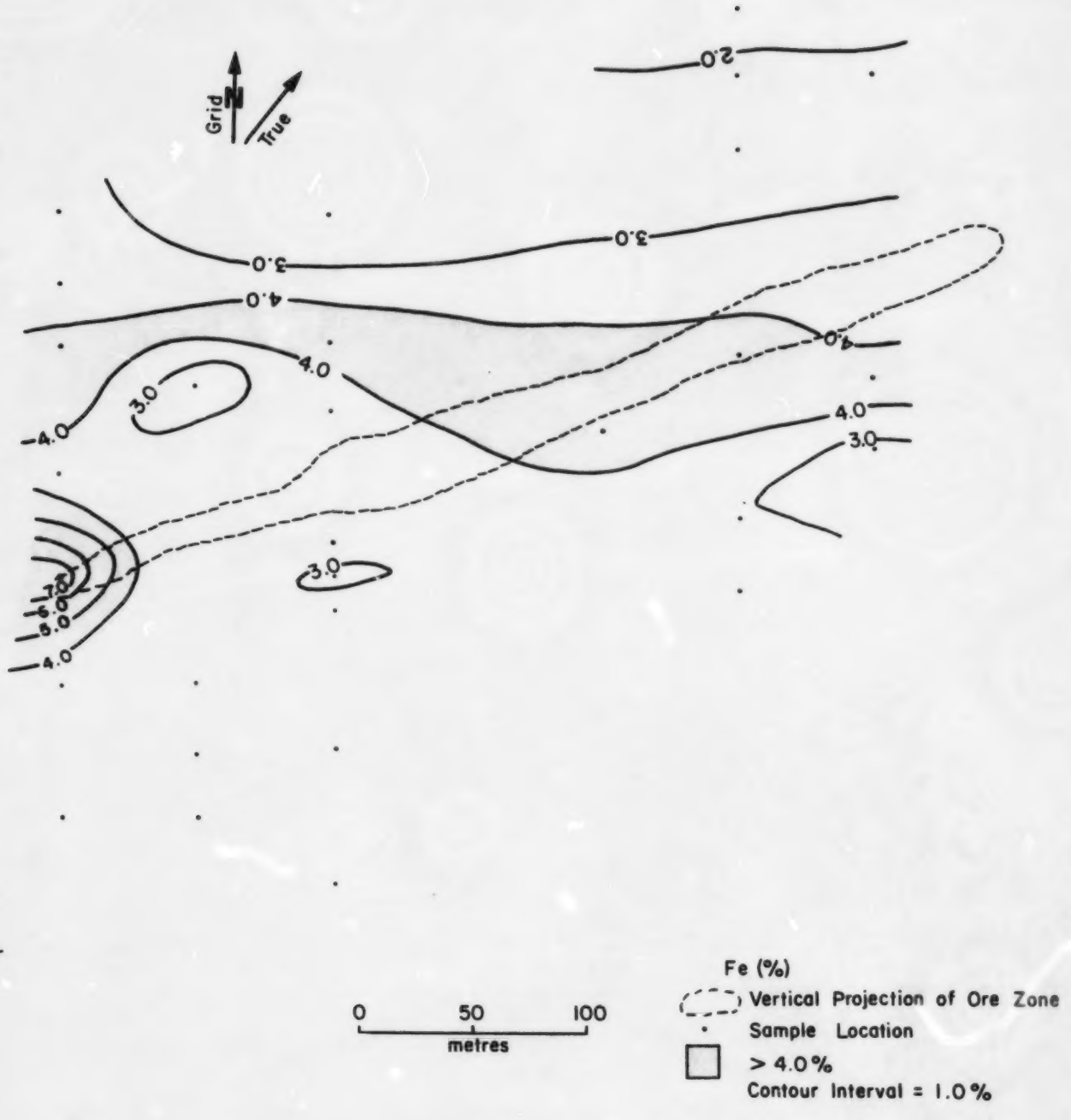

Figure 20: Contour map of Fe (%) distribution in rock samples.

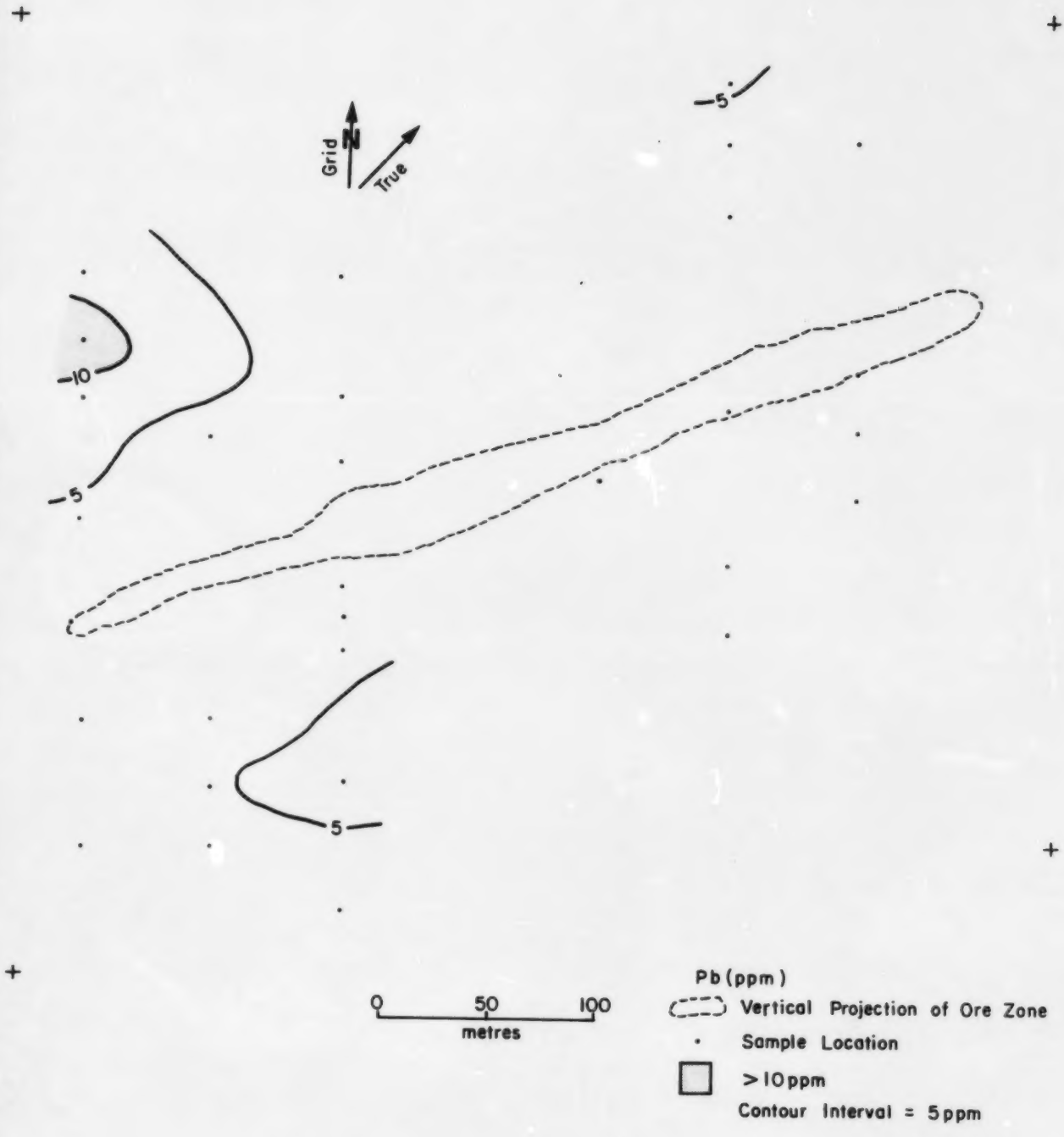

Figure 21: Contour map of Pb (ppm) distribution in rock samples.

Manganese (Fig. 22)

Four single-sample anomalies are defined: (1) 76S/96W, 640 ppm Mn; (2) 83S/96W, 812 ppm Mn; (3) 90S/92W, 528 ppm Mn; and (4) 78S/72W, 537 ppm Mn.

Zinc (Fig. 23)

The cumulative frequency curve for Zn has poorly defined inflections; the threshold value of 50 ppm Zn was chosen to delineate values above the mean (x=48 ppm Zn) and median (40 ppm Zn). Four areas with high Zn concentrations are defined: (1) a band across the north-central part of the grid (390 x 20-80 m; 51-82 ppm Zn); (2) a two-sample anomaly in the western part of the grid (140 x 60 m; 90, 129 ppm Zn); (3) a three-sample anomaly along the southwestern part of the grid (160 x 50 m; 52-64 ppm Zn); and (4) a single-sample anomaly at 72S/96W (56 ppm Zn). Only one sample, 86S/92W (129 ppm Zn), has greater than 100 ppm Zn.

GROUP 3 - High Skewness or Kurtosis ($\geq \pm$ 10.00)

Only one element, As, has skewness or kurtosis statistics $\geq \pm$ 10.00.

Arsenic (Fig. 24)

Two anomalies are defined: (1) a bilobate area in the eastern part of the grid (up to 275 x 250 m; 6-22 ppm), and (2) a single-sample anomaly at 76S/96W (6 ppm). The maximum value for As from this dataset is 22 ppm.

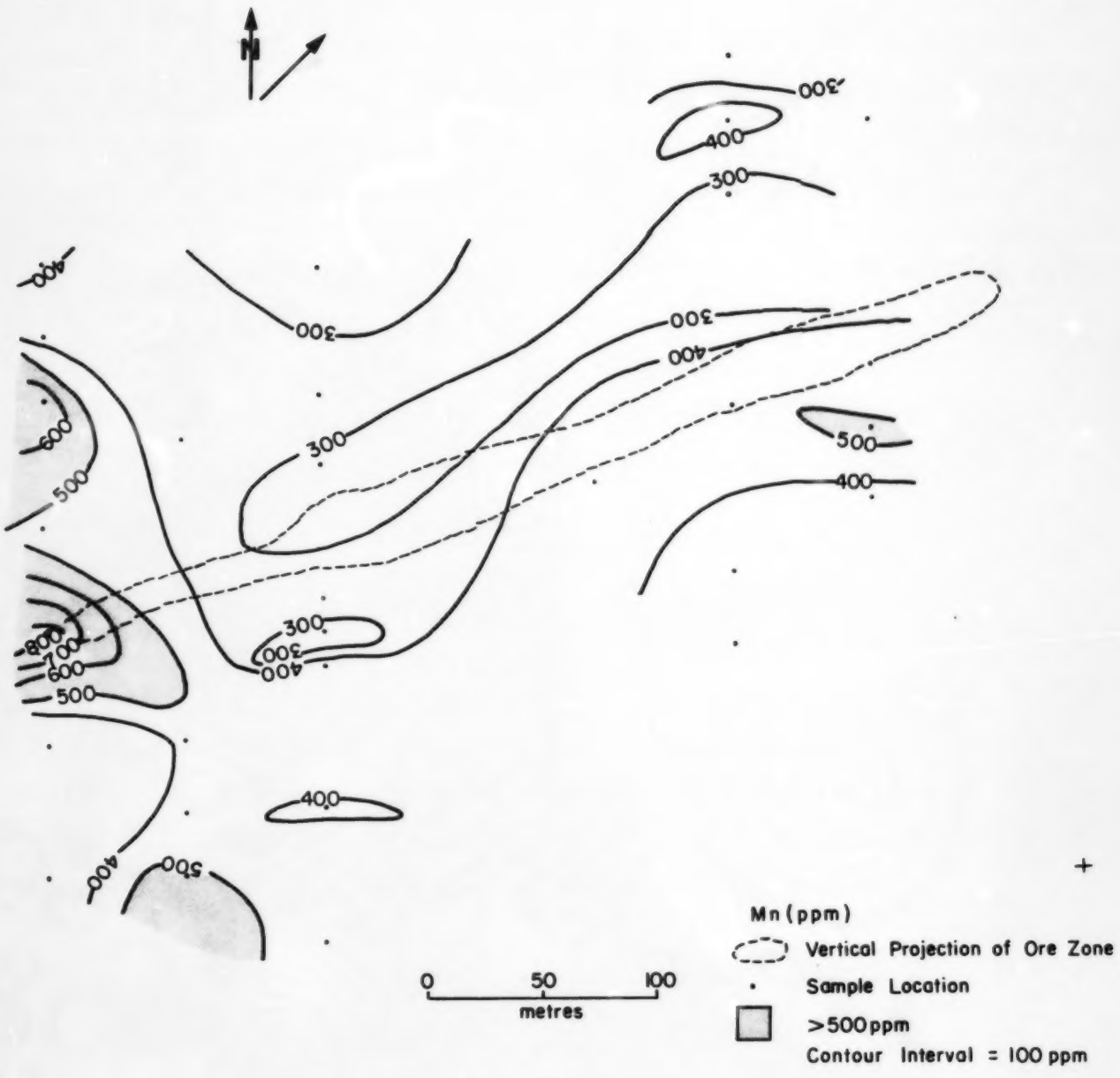

Figure 22: Contour map of Mn (ppm) distribution in rock samples.

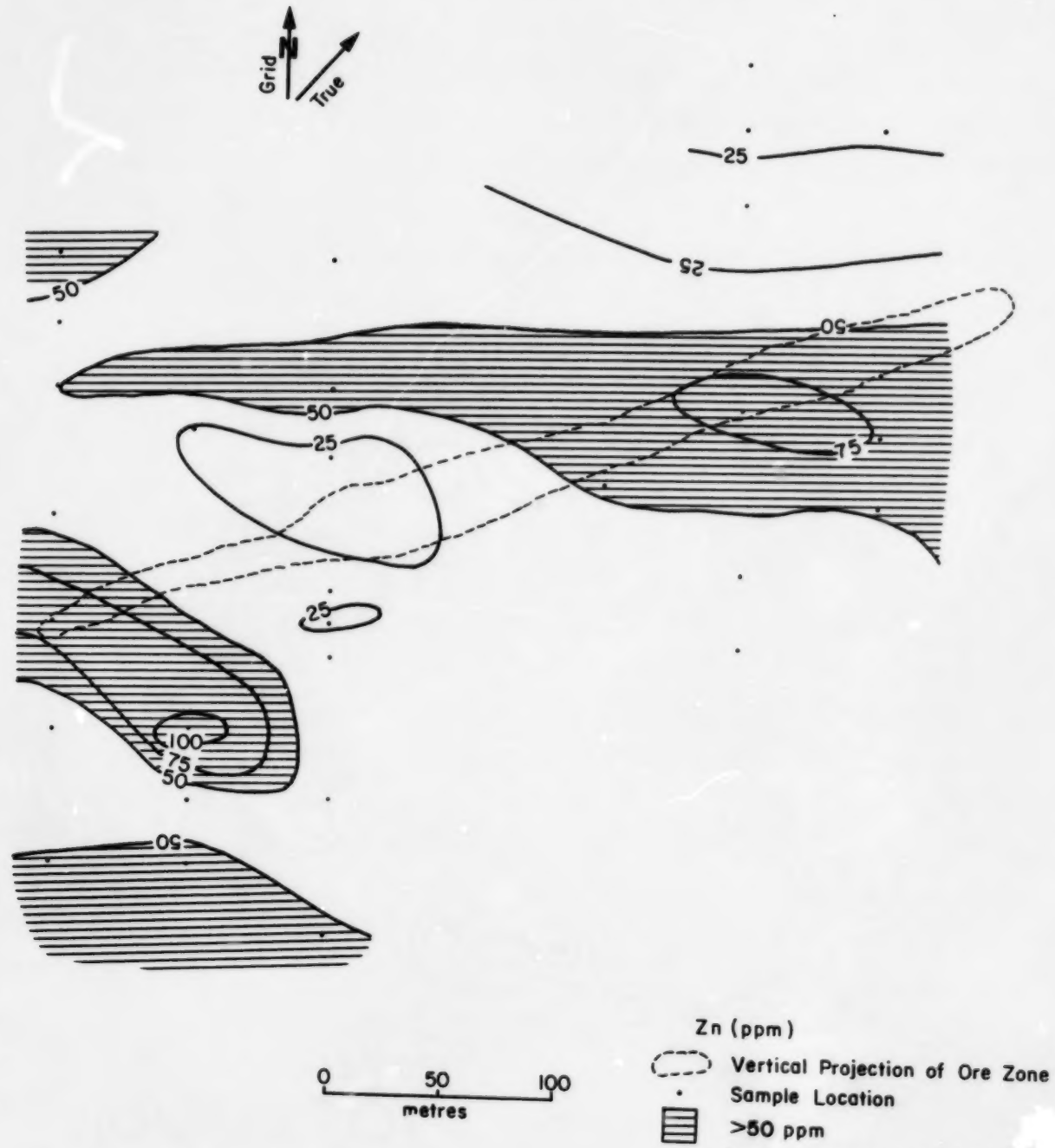

Figure 23: Contour map of Zn (ppm) distribution in rock samples.

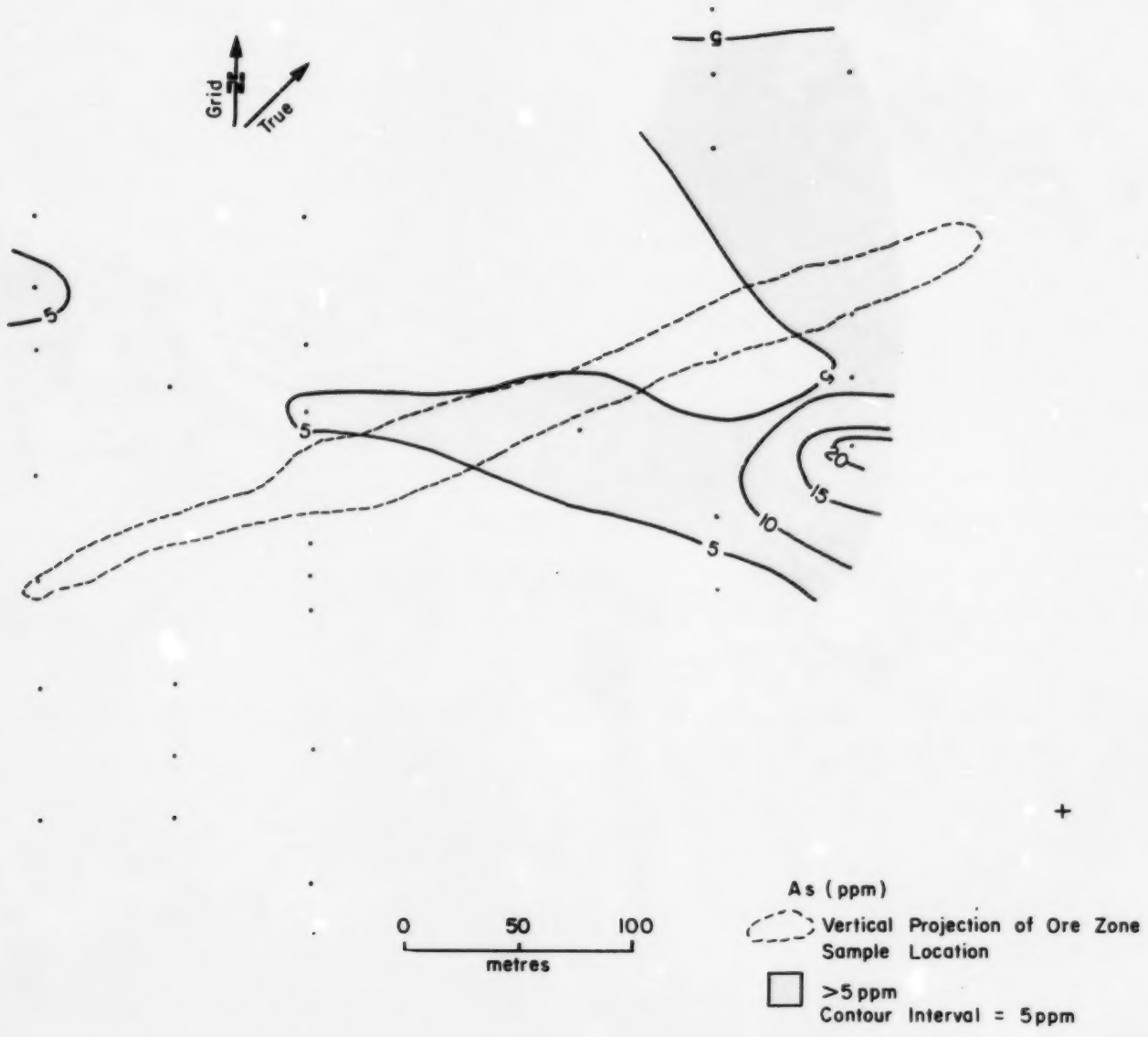

Figure 24: Contour map of As (ppm) distribution in rock samples.

DISCUSSION AND CONCLUSIONS

Sulphide Selective Dissolution

The use of a sulphide selective leach for sample dissolution was undertaken to avoid lithologic control of trace element concentrations in the dataset. None of the three predominant lithologies in the area, i.e., medium grained amphibole-feldspar porphyroblastic basalt, fine grained aphyric basalt and quartz-phyric rhyolite, are distinguishable on the basis of the derived geochemical data in Table 2 and Appendix I. This suggests, therefore, that variations within the dataset are the result of a cause-and-effect relationship between host rocks and alteration related to the mineralizing process.

Geochemical Anomalies

Many elements analyzed in this survey, viz., Al, B, Ca, Co, Cu, Na, Ni, K, Mg, P, Sr and V, have low dispersion statistics, skewness and kurtosis, and have data distributions whose cumulative frequency curves approximate a straight line. Since these data have distributions that approximate normality, they either do not properly discriminate anomalous from background values, or do so poorly. Therefore, these may have questionable value as indicators of mineralization.

The range in concentration for Au, Cu, Pb, Zn, Co, Ni and As is limited; nevertheless, low contrast anomalies were identified based on these elements. Copper, Pb and Zn contents are low despite the proximity of this area to significant massive sulphide-type mineralization and associated alteration, both at and near surface to the southwest (the No. 1 Zone) and at depth (the No. 2 Zone). It is also notable that Pb does not correlate significantly with any of the other elements in this dataset, despite the association of minor galena with Cu-Zn-Fe mineralization in the Rod deposit and with As-Cu-Fe mineralization in trenches in quartz-phyric rhyolite to the southeast. Copper and Zn values are not statistically correlatable, and locations of anomalies for these elements, as shown by contoured diagrams, are not coincident.

The southwestern part of the grid, underlain by fine grained, aphyric basalt interlayered with quartz-phyric rhyolite contains partly overlapping low-contrast anomalies that demonstrate enrichment in Cu, P, K, Ba, Zn, Mn, and depletion in Na, Ca and Sr. The fine grained aphyric basalt that is interlayered with quartz-phyric rhyolite may have these characteristics as a function of primary lithology, or these anomalies may reflect the effects of mineralization and associated alteration, possibly associated with the No. 1 Zone to the southwest. Because depletion in Na, Ca and Sr, and enrichment in Cu, Zn, K and Ba is common in areas that have been hydrothermally altered, it is likely that these rocks have also been altered.

Small areas of coincident relative depletion in Na, Ca and Sr were identified with the partial leach extraction method. These areas occur most commonly within quartz-phyric rhyolite, and are coincident with K enrichment. Another area of alkali depletion occurs along 88W, within basaltic rocks. Strontium delineates broader, higher contrast anomalies than Na or Ca in this survey.

Gold is apparently concentrated in rock samples collected from the western portion of the grid. There is a statistical correlation between Au and Ni, V, Co, and Cu, suggestive of a pyrrhotite-chalcopyrite association with Au.

Arsenic values are highest in the southeastern part of the grid, closest to the group of trenches that are mineralized with arsenopyrite. However, the trenches also contain Pb, Fe and Cu mineralization, but anomalies for these elements do not occur in this area.

Rock, Humus and Vapour Surveys

Sample number 1904, collected at 83S/96W, produced high-contrast single-sample anomalies for Mg, Co, Cu, Ni, K, V, Ba, Au, Fe, Mn and Zn. The coincidence of these anomalies at this one sample location poses the question whether this a spurious sample, possibly contaminated or an analytically nonreproducible analysis, or whether this sample indicates the presence of mineralization/alteration. Detailed mapping shows that other samples in the area consisted of basalt, whereas this sample consists of quartz-phyric rhyolite, which is interlayered with the basalt. The anomalies may reflect these different lithologies, however other samples collected from the quartz-phyric rhyolite (e.g., sample numbers 1911, 1912) do not exhibit the same anomalous responses. Humus samples also show multi-element (Cu, Zn, Co, Ni, Fe, Mn, and specific conductance) anomalies in the same general area (Ferreira and Fedikow, 1988; Ferreira and Fedikow, 1990), suggesting that this sample did produce results correlatable with other media, possibly indicative of mineralization and alteration in the area.

The highly unusual chemical nature of sample 1904 (i.e., single sample anomalies for eleven major and trace elements) may be explained in terms of the attitude of the orebody and associated alteration. The western end of the No. 2 zone is situated 183 m below surface, whereas the eastern end is 732 m deep. It is possible that sample 1904 has marked the alteration associated with the end of the No. 2 zone that is closer to surface. The areal distribution of many of the anomaly forming elements is also supportive of this observation (cf., Fig. 16, 18 and 19).

Humus samples also show multi-element (Cu, Zn, Co, Ni, Fe, Mn, and specific conductance) anomalies in the southwestern area of the grid (Ferreira and Fedikow, 1988, 1990). However, the anomalies are only partly spatially overlapping with rock geochemical anomalies in this area, and the suite of elements that are anomalous are not identical for the two media. Because the locations of sample stations are not identical for the humus samples and the rock samples, some differences in the locations of anomalies is expected. As well, analyses of humus samples may reflect

the transfer of elements from depth by electrochemical dispersion and meteoric water transport (Govett, 1973, 1976; Nuutilainen and Peuraniemi, 1977), not simply the effects of weathering of nearby outcrops; thus, the humus geochemical anomalies may indicate proximal concentrations of these elements, namely, those delineated in the rock geochemical anomalies, or they may indicate mineralization at depth, or a combination of these two potential sources of mineralization.

Although the results of the mercury vapour survey were difficult to interpret because of very poor reproducibility, there appears to be a weak spatial correlation with some of the elements determined for rock samples in this study. The majority of anomalous mercury vapour concentrations were measured from samples collected on the southern portion of the grid. This is in broad agreement with the results of Al (Fig. 6), Cu (Fig. 10), P (Fig. 13), K (Fig. 14), Sr (Fig. 16), V (Fig. 17), Ba (Fig. 18) and Zn (Fig. 23), all of which form areally more extensive anomalies in rock samples collected from the same area.

CONCLUSIONS

Multiple low-contrast rock geochemical anomalies were identified in the survey area based on an aqua-regia partial dissolution of outcrop chip samples. The areal distribution of the anomalies, as well as the limited range of concentrations within these anomalies, may be a function of the attitude and depth of burial of the No. 2 zone. Broad agreement exists between the results of rock, humus and possibly vapour geochemical results from this study area.

The results of the rock geochemical survey, as well as of the humus geochemical survey (Ferreira and Fedikow, 1988; Ferreira and Fedikow, 1990), indicate that the grid area used for sampling and mapping needs to be expanded in order to make conclusive statements about sources and extent of mineralization and related alteration, and the role of lithologies in controlling the geochemistry of trace elements in rocks and other sampling media. In particular, sampling needs to be expanded to the southwest to cover the area of the No. 1 Zone, and to the southeast to cover the area marked by numerous mineralized trenches in quartz-phyric rhyolite. This would address, in part, the possible dislocation of alteration zones by deformation that would have effectively removed altered rocks from the immediate vicinity of the deposit and grid sample locations.

ACKNOWLEDGMENTS

The authors wish to acknowledge the cooperation of T. Baumgartner and J. Kitzler from Hudson Bay Exploration & Development Co. Ltd. and D. Ziehlke of Pro Roc Exploration Ltd., and to thank them for information and valuable discussions. C. Roney collected the rock samples. C. Malis, A. Lebedynski and K. Cooley assisted in field mapping. C. Sandy, G. Foote, and N. Barton drafted the geochemical contour diagrams. G. Conley produced the cumulative frequency diagrams. G.H. Gale, W.D. McRitchie and D.A. Baldwin provided constructive criticism and editorial review.

REFERENCES

Bailes, A.H.

1971: Preliminary compilation of the geology of the Snow Lake-Flin Flon-Sherridon area; Manitoba Department of Mines and Natural Resources, Mines Branch, Geological Paper 71/1, 27 p.

Bruce, E.L.

1918: Amisk-Athapapuskow Lake district; Geological Survey of Canada, Memoir 105, 91 p.

Bailes, A.H., Syme, E.C., Galley, A., Price, D.P., Skirrow, R. and Ziehlke, D.J.

1987: Early Proterozoic volcanism, hydrothermal activity, and associated ore deposits at Flin Flon and Snow Lake, Manitoba; Geological Association of Canada, Field Trip Guidebook, Trip 1, 95 p.

Coats, C.J.A., Clark, L.A., Buchan, R. and Brummer, J.J.

1970: Geology of the copper-zinc deposits of Stall Lake Mines Ltd., Snow Lake area, northern Manitoba; Economic Geology, v. 65, p. 970-874.

Fedikow, M.A.F.

1986: Mercury gas surveys over base and precious metal mineral deposits in the Lynn Lake and Snow Lake areas, Manitoba; Manitoba Energy and Mines, Open File Reports OF85-11, 45 p.

Fedikow, M.A.F. and Ferreira, K.J.

1987: Results of a rock geochemical survey of the Lynn Lake Rhyolitic Complex; Manitoba Energy and Mines, Open File Report OF87-6, 27 p.

Fedikow, M.A.F. and Amor, S.

1990: Evaluation of a mercury-vapour detection system in base- and precious-metal exploration, northern Manitoba; Journal of Geochemical Exploration, v. 38, p. 351-374.

Ferreira, K.J. and Fedikow, M.A.F.

1988: Preliminary results of a humus geochemical survey over the Rod Cu-Zn deposit, Snow Lake, Manitoba; Manitoba Energy and Mines, Open File Report OF87-12, 35 p.

Ferreira, K.J. and Fedikow, M.A.F.

1990: Specific conductance and hydrogen ion concentration as indicators of trace element geochemical response in humus: Rod Cu-Zn and Big Island Zn-Cu-Au deposits, Manitoba; Journal of Geochemical Exploration, v. 37, p. 185-203.

Gale, G.H. and Koo, J.

1977: Evaluation of massive sulphide environments; In Canada-Manitoba Non-renewable resource evaluation program (NREP), 2nd Annual Report 1976-1977, p. 43-62.

Tennant, C.B. and White, M.L.

1959: Studies of the distribution of some geochemical data; Economic Geology, v. 54, p. 1281-1291.

Walford, P.C. and Franklin, J.M.

1982: The Anderson Lake Mine, Snow Lake, Manitoba; In Precambrian sulphide deposits (R.W. Hutchinson, C.D. Spence, J.M. Franklin, ed.); Geological Association of Canada, Special Paper 25, p. 481-523.

APPENDIX I: ANALYTICAL DATA, ROCK GEOCHEMICAL SAMPLES, ROD DEPOSIT AREA

Sample Number	Mo ppm	Cu ppm	Pb ppm	Zn ppm	Ag ppm	Ni ppm	Co ppm	Mn ppm	Fe %	As ppm	U ppm	Th ppm	Sr ppm	Cd ppm
71-86-1901	2	91	7	56	0.1	8	4	402	3.21	4	5	1	46	1
71-86-1902	2	62	13	45	0.1	7	7	373	3.39	6	5	1	34	1
71-86-1903	1	197	8	50	0.3	12	17	640	4.51	4	6	2	39	1
71-86-1904	1	103	4	44	0.1	10	13	474	3.89	4	6	3	146	1
71-86-1905	1	159	5	90	0.2	13	20	812	7.76	2	5	3	16	1
71-86-1906	1	77	2	34	0.1	9	10	353	3.27	2	5	1	56	1
71-86-1907	1	39	2	52	0.1	8	8	366	3.53	4	5	2	10	1
71-86-1909	1	171	3	24	0.1	9	10	374	2.83	2	5	1	3	1
71-86-1910	2	197	3	129	0.1	10	12	404	3.46	2	5	2	82	1
71-86-1911	1	137	4	37	0.1	9	11	407	3.29	2	5	2	21	1
71-86-1912	2	26	2	64	0.1	5	10	528	3.47	2	5	2	7	1
71-86-1913	2	35	3	56	0.1	8	8	487	3.70	2	5	2	17	1
71-86-1914	2	110	7	36	0.2	10	11	395	3.34	2	6	2	164	1
71-86-1915	1	101	4	37	0.2	10	12	445	3.60	2	7	2	51	1
71-86-1916	1	97	5	24	0.2	9	8	289	2.83	2	7	2	166	1
71-86-1917	1	171	3	26	0.2	9	11	320	3.46	2	5	2	108	1
71-86-1918	1	131	3	22	0.1	11	13	272	3.69	6	5	1	2	1
71-86-1919	1	106	2	68	0.1	9	8	395	4.22	2	5	1	5	1
71-86-1920	2	152	3	34	0.1	6	4	224	2.30	2	5	1	41	1
71-86-1922	1	101	5	54	0.1	10	14	468	4.59	8	5	1	12	1
71-86-1923	1	76	4	43	0.1	10	11	387	3.12	3	5	1	6	1
71-86-1924	1	51	2	38	0.1	12	6	357	3.01	8	5	2	5	1
71-86-1925	2	142	5	82	0.1	9	11	461	4.86	2	5	1	17	1
71-86-1926	1	99	2	18	0.2	11	7	294	2.08	7	5	1	125	1
71-86-1927	1	116	2	30	0.2	10	9	425	2.60	8	6	2	55	1
71-86-1928	1	78	6	34	0.1	11	6	202	1.44	3	5	1	96	1
71-86-1929	2	54	4	51	0.1	13	4	377	2.96	22	5	1	8	1
71-86-1930	2	112	5	74	0.1	4	10	537	4.85	6	5	1	7	1
71-86-1931	2	71	3	70	0.2	5	9	424	3.71	8	5	2	7	1
71-86-1932	1	77	3	26	0.2	6	6	318	2.17	7	5	1	29	1

Sb ppm	Bi ppm	V ppm	Ca %	P %	La ppm	Cr ppm	Mg %	Ba ppm	Ti %	B ppm	Al %	Na %	K %	W ppm	Au ppb
2	2	11	2.31	0.022	3	9	0.62	44	0.06	13	2.18	0.17	0.17	1	1
2	2	30	2.04	0.021	4	7	0.83	72	0.09	14	3.23	0.31	0.39	2	3
2	2	133	4.20	0.016	3	10	0.92	50	0.11	12	4.27	0.26	0.20	4	24
2	2	113	3.65	0.052	5	17	1.24	131	0.12	17	4.13	0.68	0.37	1	7
2	2	206	2.93	0.065	7	23	1.81	554	0.22	2	2.06	0.28	0.95	1	15
2	2	76	1.75	0.063	6	14	1.08	98	0.07	19	2.09	0.26	0.24	3	3
2	2	52	0.39	0.029	4	6	0.77	321	0.13	10	1.30	0.09	0.61	1	1
2	2	75	1.54	0.012	2	8	0.92	59	0.06	2	1.22	0.12	0.16	1	20
2	2	90	2.34	0.055	6	17	1.13	141	0.09	15	2.47	0.33	0.27	1	38
2	2	96	1.59	0.054	6	18	1.04	111	0.10	7	1.68	0.25	0.21	3	6
2	2	54	0.31	0.031	6	4	0.87	427	0.16	8	1.43	0.09	0.97	1	1
2	2	55	0.83	0.029	5	6	0.78	329	0.13	10	1.55	0.15	0.77	2	4
2	2	91	2.80	0.056	6	18	0.97	149	0.09	11	3.23	0.48	0.30	2	9
2	2	116	2.18	0.064	4	15	1.15	166	0.12	11	2.31	0.36	0.32	2	1
2	2	74	3.01	0.050	5	15	0.78	42	0.06	12	3.39	0.54	0.12	3	1
2	2	86	2.50	0.056	6	17	0.97	68	0.07	11	2.89	0.38	0.24	1	12
3	2	171	0 55	0.020	2	9	0.57	3	0.04	4	0.65	0.08	0.01	3	16
2	2	15	0.80	0.038	3	5	0.77	77	0.15	7	1.48	0.09	0.54	1	1
2	2	6	1.02	0.034	3	6	0.34	25	0.06	8	1.16	0.13	0.08	2	1
2	2	103	1.68	0.035	2	6	1.23	54	0.12	2	1.94	0.19	0.35	1	6
2	2	74	0.55	0.025	4	8	0.95	202	0.11	8	1.26	0.11	0.57	2	2
2	2	18	0.48	0.033	4	20	0.36	108	0.10	3	0.67	0.09	0.37	2	7
2	2	82	1.23	0.036	3	8	1.26	136	0.16	6	2.56	0.23	0.60	1	1
2	2	52	3.68	0.012	2	28	0.81	58	0.05	15	3.86	0.42	0.07	1	1
2	2	90	5.42	0.015	2	15	0.83	24	0.09	22	5.46	0.57	0.08	5	2
2	2	51	5.90	0.046	3	26	0.42	132	0.17	22	6.08	0.53	0.12	3	1
2	2	15	1.33	0.024	5	13	0.49	106	0.07	10	0.97	0.07	0.31	1	8
2	2	21	1.87	0.041	4	3	0.75	125	0.20	6	1.96	0.17	0.75	2	3
3	2	29	1.16	0.035	3	6	0.67	110	0.16	6	1.42	0.07	0.66	2	1
2	2	63	2.43	0.028	2	14	0.5	11	0.09	7	2.54	0.42	0.05	2	3

APPENDIX II: Histograms of analytical data for individual elements.

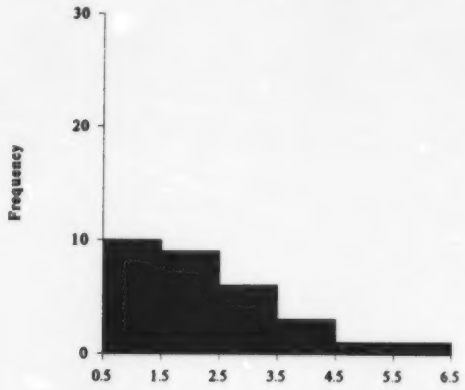

Al. %

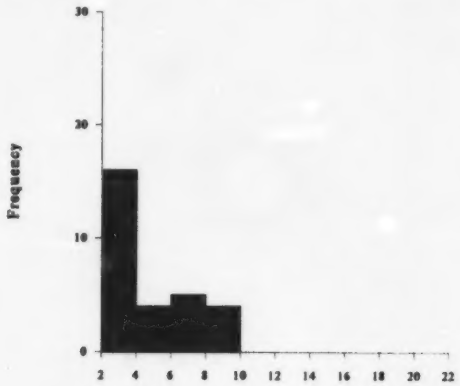

As. ppm

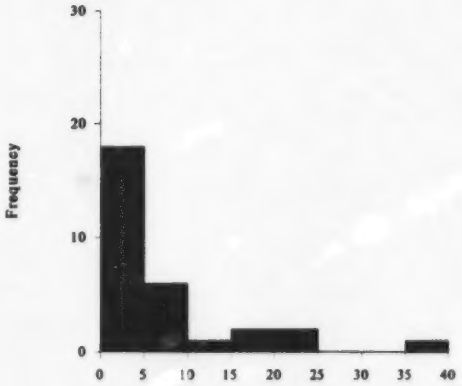

Au. ppb

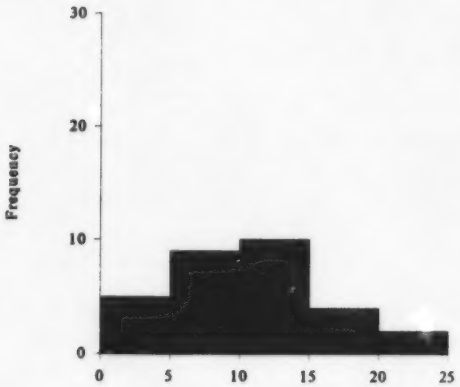

B. ppm

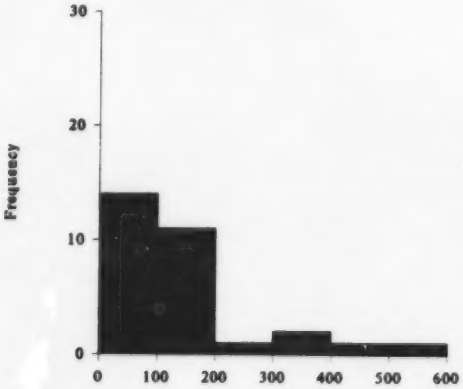

Ba. ppm

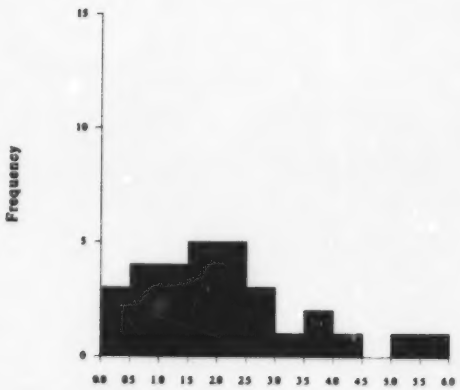

Ca. %

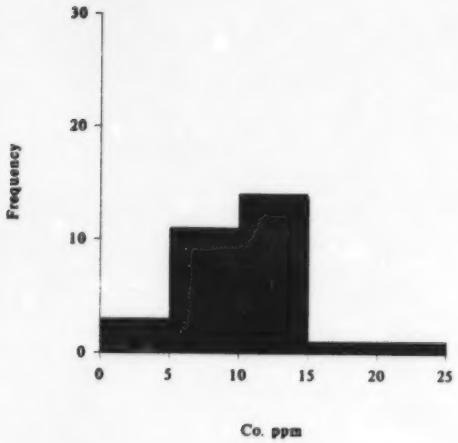
Frequency
30
20
10
0
0 5 10 15 20 25
Co. ppm

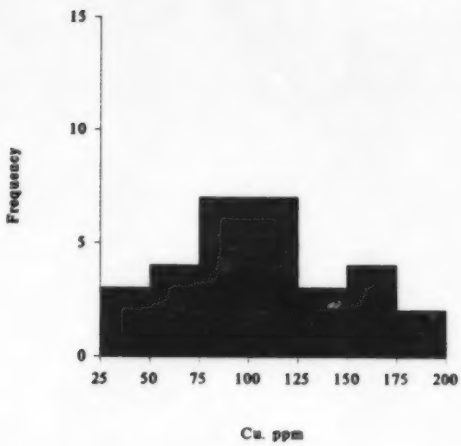
Frequency
15
10
5
0
25 50 75 100 125 150 175 200
Cu. ppm

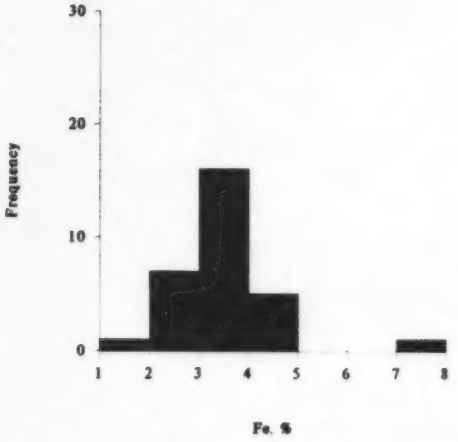
Frequency
30
20
10
0
1 2 3 4 5 6 7 8
Fe. %

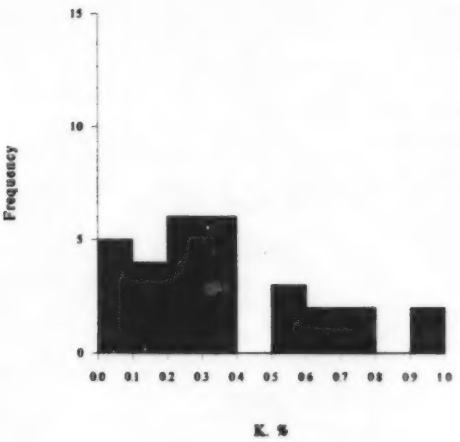
Frequency
15
10
5
0
00 01 02 03 04 05 06 07 08 09 10
K. %

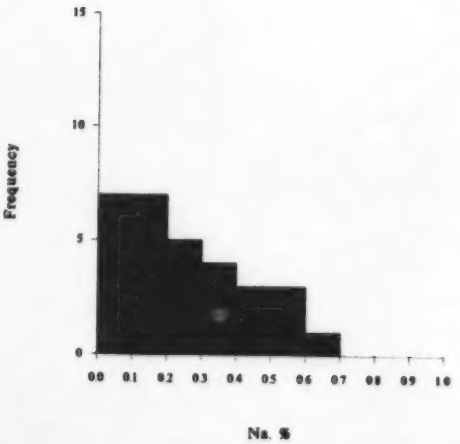
Frequency
15
10
5
0
00 01 02 03 04 05 06 07 08 09 10
Na. %

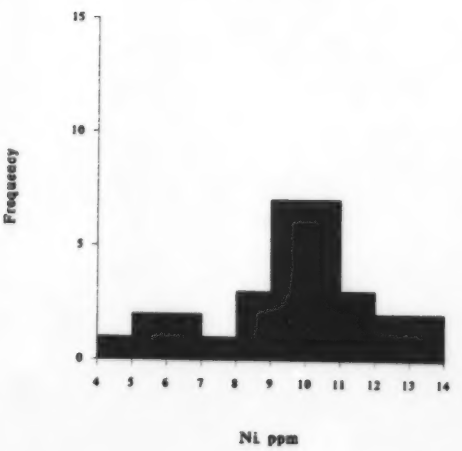
Frequency
15
10
5
0
4 5 6 7 8 9 10 11 12 13 14
Ni ppm

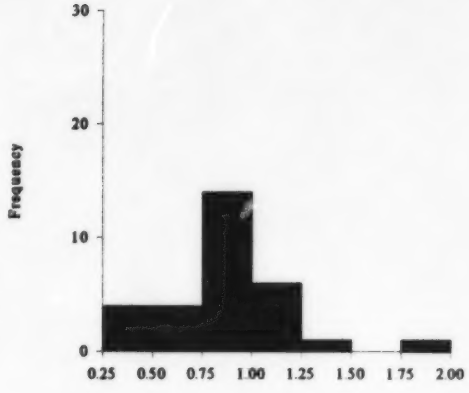
Frequency
30
20
10
0
0.25 0.50 0.75 1.00 1.25 1.50 1.75 2.00
Mg. %

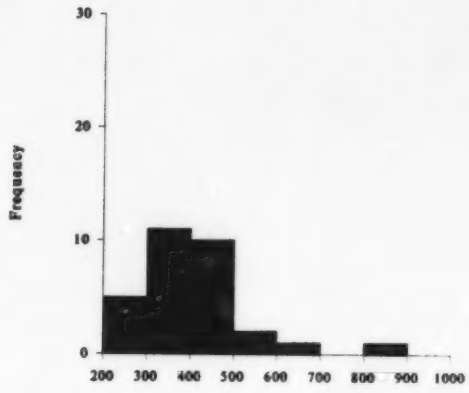
Frequency
30
20
10
0
200 300 400 500 600 700 800 900 1000
Mn. ppm

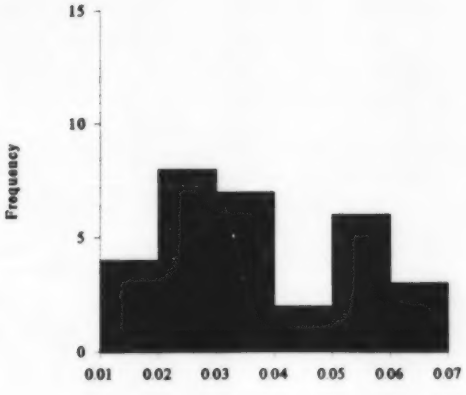
Frequency
15
10
5
0
0.01 0.02 0.03 0.04 0.05 0.06 0.07
P. %

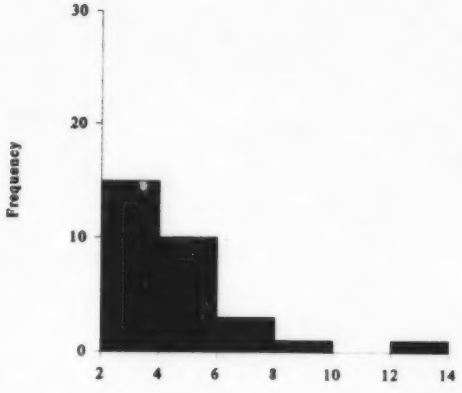
Frequency
30
20
10
0
2 4 6 8 10 12 14
Pb. ppm

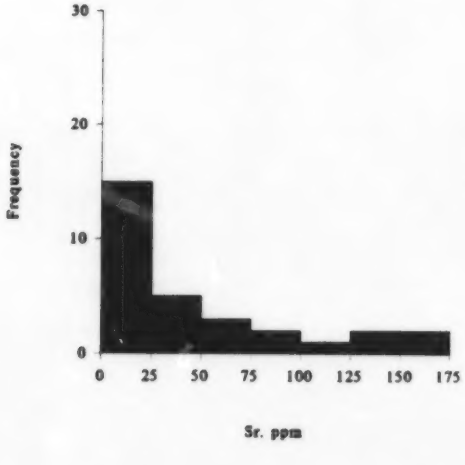
Frequency
30
20
10
0
0 25 50 75 100 125 150 175
Sr. ppm

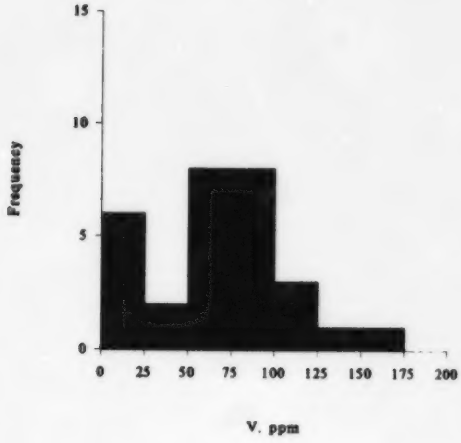
15
10
5
0
Frequency
0
25
50
75
100
125
150
175
200
V. ppm

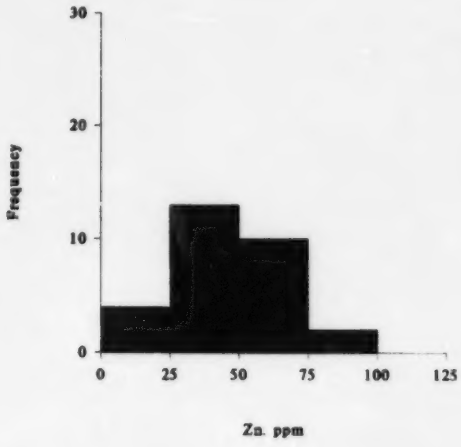
30
20
10
0
Frequency
0
25
50
75
100
125
Zn. ppm